OBSERVATIONS OF THE SPATIAL STRUCTURE OF INTERSTELLAR HYDROGEN. I. HIGH-RESOLUTION OBSERVATIONS OF A SMALL REGION*

CARL HEILES†

Princeton University Observatory

Received March 27, 1967; revised May 23, 1967

ABSTRACT

The 21-cm line radiation emitted by low-velocity neutral hydrogen has been mapped in detail in the region bounded by $l^{II} \simeq 100°–140°$, $b^{II} \simeq 13°–17°$, using the 300-foot telescope and the 100-channel autocorrelation receiver at the National Radio Astronomy Observatory in Green Bank. The beam width of the antenna at this wavelength is 10′, the velocity resolution about 1 km/sec, the total range of velocities observed about 50 km/sec, and the antenna temperature sensitivity about 1°.

Several considerations lead to the adoption of a common distance of 500 pc to all of the hydrogen as a reasonable approximation. The gas can be resolved into three physical components: a diffuse, smooth background, contributing about $\frac{3}{4}$ of the integrated 21-cm emission; and two large sheets of gas having relative motion in which the hydrogen density is probably about two atoms/cm^3, which contain structure. In part of the region the sheets coexist in space and velocity. The velocity of each sheet is highly ordered over distances of tens of degrees on the sky; linear structures characterized by no hydrogen ("rifts") run across each sheet. The disturbance responsible for the rifts probably exists in sheetlike form, too.

The present observations do not correspond at all with the predictions of the "standard cloud model." Concentrations of gas which one might call clouds are present in the sheets, but usually their density is no larger than twice the surrounding density; about ten of these objects exist, some of which are so large that the tidal force of the galactic gravitational field must affect their equilibrium. Especially prominent are the "group clouds" which are similar to classical "interstellar clouds" but which are clumped together into two groups; much of the large velocity dispersion of these objects may result from systematic radial motion. No enhanced 21-cm emission is observed at positions of dense dust clouds; this is attributed to the presence of cold or molecular hydrogen in these objects, which are bound by self-gravitation if the optical extinction is from classical dielectric spheres.

Small concentrations of near stellar mass, distinctly different from the above concentrations, are observed in profusion; but since they are small they contain only about 10 per cent of the mass of the sheets. Typical radii of these "cloudlets" are a few parsecs; excess densities are not large, about a factor 2. The upper limit to the kinetic temperature implied by their velocity width is about 100° K.

The highest brightness temperature observed in the region is 130°, equal to the commonly accepted value for the kinetic temperature in the galactic plane; the line profile does not appear saturated. This, together with previous determinations of kinetic temperature, implies the existence of large temperature variations in the interstellar gas.

The decrease of the number of hydrogen atoms/cm^2 in the line of sight with increasing galactic latitude is much faster than $1/\sin b$; the decrease near latitude 28° is almost discontinuous. The conclusion follows that in this region little hydrogen exists in the neighborhood of the Sun.

I. INTRODUCTION

It is the patchy appearance of interstellar absorption that probably first led to the concept that the interstellar medium is composed of "clouds." The specification of general cloud parameters from photographs of dust clouds is based upon the assumption that the gas and dust are intimately associated. We believe that dust clouds must contain gas. If they do not, the dust clouds represent regions of very anomalous chemical abundance. On the other hand, the existence of gas does not require the presence of dust; gas structures may exist which contain no dust. Support for the cloud concept can also be obtained from photographs of glowing gas near hot stars, but here the gas is af-

* Based in part on a thesis submitted to Princeton University in partial fulfilment of the Ph.D. degree.

† Present address: Berkeley Astronomy Department, University of California.

fected dynamically by the hot stars and, more important, the nearby interstellar matter has just been in that peculiar state in which it is able to contract to form the young, hot stars.

"Typical" interstellar matter can be observed using optical absorption lines and also the 21-cm radio line of neutral hydrogen. Optical absorption line spectra (see Adams 1949; Münch 1957) usually consist of several very narrow, well-separated lines; this structure seems to imply that the gas is distributed in clouds which have small internal velocity dispersions but which move relatively rapidly with respect to one another. Radio astronomers (van Woerden, Takakubo, and Braes 1962; hereinafter denoted as "WTB") observed emission profiles of the 21-cm line at discrete points in the sky in intermediate galactic latitudes and deduced characteristic parameters of clouds by carefully resolving the spectra into Gaussian components (see Blaauw 1962; Takakubo 1963; Takakubo and van Woerden 1966). Similar analyses have been performed on absorption profiles of radio sources in the galactic plane (see Clark, Radhakrishnan, and Wilson 1962; Clark 1965).

Because the positions at which these spectra are recorded are separated by at least a few degrees, no map of the small-scale structure of the interstellar gas is available. Such analyses thus constitute indirect measurements of the parameters of the supposed clouds, and have been alternately interpreted (Donn 1958) as velocity "streams." The only way to prove that interstellar line and 21-cm components indeed belong to clouds is to map their spatial structure; none of the above data is *direct* evidence for the applicability of the cloud concept to the majority of the interstellar gas.

On occasion optical astronomers have been able to define a cloud spatially. Münch and Unsöld (1962) found a high-velocity optical absorption line with well-defined boundaries; they estimated its diameter as 1 parsec and its density as 1.5 hydrogen atoms/cm^3. Schlüter, Schmidt, and Stumpff (1953) were able to define the approximate boundaries of a larger cloud from Adams' (1949) data.

Radio astronomers have the means to produce spatial maps of the structure of interstellar gas because they can observe the density of the interstellar medium directly through the 21-cm line of neutral hydrogen; but the complete mapping of a large region is very time-consuming unless a multichannel receiver and automatic reduction methods are available. Such observations should not be made in the galactic plane because we must distinguish small-scale structure from all the other hydrogen in the line of sight. Van Woerden (1962) and Dieter (1964, 1965) have made maps of the required quality. Dieter mapped regions near the galactic poles. She found that spatial structure could be represented by clouds typically having the following parameters: diameter = 10 parsecs, density = 2 hydrogen atoms/cm^3, mass = 20 solar masses, and internal velocity dispersion = about 2 km/sec. Although these observations were taken in rather special directions, the results are probably the first for interstellar matter which can be a priori assumed to be typical, because van Woerden observed near the Orion Nebula.

The antenna beam used by Dieter was quite broad—about 1°. WTB, who used a larger antenna, found evidence for the existence of structure smaller than their antenna beam width; Takakubo (1963) has frustratedly remarked that the minimum angular size of observed objects may always be the size of the antenna beam. The need for a detailed map of the largest feasible area of the sky using the largest available telescope is thus apparent. The present study is an attempt to fulfil this need. About 160 square degrees of sky at intermediate galactic latitude (b^{II} = 13°–17°) were mapped in detail using the 300-foot telescope at Green Bank and a receiver providing velocity resolution expected to be great enough to resolve all profile components. The longitude boundaries of the region, l^{II} = 100°–140°, were chosen for convenience.

The original data are published in a catalogue (Heiles 1966*a*), available in limited quantities for distribution to interested parties. The present paper constitutes the author's interpretation of the data in that catalogue. The author has especially attempted to convey a reliable *qualitative* picture of the interstellar medium as revealed by these observations, keeping in mind the spirit of the comments by Spitzer (1958), which should be remembered by every worker in this field.

II. EQUIPMENT AND TECHNIQUES

The observations were made during two sessions (December, 1964; hereafter denoted as the first observing period; and May, June, and July, 1965, hereafter denoted as the second observing period) with the 300-foot transit telescope (Findlay 1963) and the 100-channel autocorrelation receiver (Shalloway 1964) of the National Radio Astronomy Observatory.

a) Antenna

The half-power beam width (HPBW) of the 300-foot antenna at the operating frequency and with the feeds used is 10′. Different feeds were used for the two observing periods; the resulting aperture efficiencies (η_a; for a discussion of antenna parameters see Ko 1961) were different, and were measured by H. Wendker to be 0.37 during the first observing period and 0.42 during the second. The associated beam solid angle efficiencies (η_B, often called simply beam efficiency) are 0.49 and 0.56, respectively. These numbers refer only to the situation of the antenna pointing toward the zenith (declination approximately 38°). The efficiencies become smaller when the antenna is moved from this position because of surface deformation. This effect has been measured by I. Pauliny-Toth (private communication), and it reduces the aperture efficiencies quoted above by 0.925 at declination 74°. All of the observations discussed in this paper were treated as though the aperture efficiency was reduced by this factor, even though the efficiencies change by about ± 4 per cent throughout the declination range in the observed region in which $\delta = 68°$ to 80°.

When checking the adopted temperature scale on G. Westerhout's (private communication) observations of the galactic anticenter, the author found that the use of the above efficiencies led to average values of over 200° K for the typical peak profile temperatures, which is much higher than the 125° K adopted by most workers (see van de Hulst, Muller, and Oort 1954; Kerr, Hindman, and Gum 1959). Further investigation disclosed that no real discrepancy exists because the angular response of the 300-foot antenna can be decomposed into two beams: the primary beam, to which the parameters given above apply; and a second "error beam," roughly Gaussian in shape, due to the surface irregularities of the dish (Mezger 1963; Baars and Mezger 1964).

The total response of the secondary beam relative to that of the primary beam can be easily calculated by remembering that, to conserve energy, the integral of the directive gain over all directions must equal 4π; but the integral of the directive gain over the solid angle subtended by the primary beam is only $\eta_B \times 4\pi$, so that most of the remainder is accounted for by the response of the error beam. However, part of the remainder is contributed from diffraction lobes, ohmic losses, and (especially) "spillover" radiation occurring because the feed sees the ground outside the rim of the dish. We take these latter contributions to be $0.095 \times 4\pi$. (This numerical value depends upon the amount of spillover radiation, which in turn depends on the feed used. The value quoted is the result of measurements of aperture efficiency as a function of wavelength made by Mezger [1963]; we assume that $\eta_a/\eta_b = 0.74$.) Thus the "error beam solid angle efficiency" is about 0.4—almost equal to that of the main beam. That is, when observing extended features which fill the error beam (such as neutral hydrogen) nearly half of the power delivered to the receiver results from emission outside of the primary beam. Any decrease in the main beam solid angle efficiency (as occurs, e.g., when the telescope is pointed away from the zenith) is matched by a corresponding increase in the integrated contribution from the error beam.

The error beam can be described approximately by a Gaussian function having a

HPBW of 2.57° (Baars and Mezger, 1964). Thus the antenna temperature ($T_{a(\theta_0,\phi_0)}$) for a given frequency measured when pointing the telescope in the direction (θ_0,ϕ_0) is

$$T_{a(\theta_0,\phi_0)} = \frac{1}{4\pi} \int\int D_{(\theta-\theta_0,\phi-\phi_0)} T_{b(\theta,\phi)} \, d\theta d\phi \, , \tag{1}$$

where $T_{b(\theta,\phi)}$ is the brightness temperature at the given frequency at position (θ,ϕ); the directive gain, D, was approximated for all of the present observations (η_B was taken as 0.502 and the contribution from the spillover radiation was taken as 0.095 × 4π for both observing sessions even though different feeds were used) to be

$$\frac{D_{(\theta,\phi)}}{4\pi} = \frac{0.502}{\pi\sigma_1^2} \exp - \left(\frac{\theta^2+\phi^2}{\sigma_1^2}\right) + \frac{0.403}{\pi\sigma_2^2} \exp - \left(\frac{\theta^2+\phi^2}{\sigma_2^2}\right). \tag{2}$$

The first term on the right-hand side is from the primary beam, for which $\sigma_1 = 6'$; the second, from the error beam, and $\sigma_2 = 96'$. The expression for the contribution from the error beam, valid for an ensemble average of telescopes having ideally distributed surface irregularities, is a poor approximation for one real antenna. For example, the angular distribution of the error beam is known not to be circularly symmetric, especially at large zenith angles.

The brightness temperature at a given frequency is related to the antenna temperature by

$$T_b = T_a/\eta \, , \tag{3}$$

where η is an effective beam solid angle efficiency. Its value, which must be calculated for every feature from equations (1) and (2), is 0.502 for a small object and 0.905 for an object large compared to the width of the error beam. In particular, the "correct" value for general hydrogen-line work—e.g., comparison with results of other observers—is 0.905, because the gross distribution of hydrogen changes little over angles of 3° except near the galactic plane.

It is interesting to notice that the response of the real 300-foot antenna can be described crudely as the response from a perfect 300-foot antenna averaged together with the response from the 7.5-meter Kootwijk antenna used for the first large-scale survey of the galactic plane (van de Hulst *et al.* 1954).

The effect of the error beam in hydrogen absorption work cannot be neglected if accurate results are to be derived. Moreover, the effect of the error beam is also important in continuum extended source work, particularly so when measuring polarization because the error beam is randomly polarized relative to the main beam. Of course, the error beam has little effect on the measurements of point source fluxes because of its large HPBW.

The positional error calibration of the antenna was performed by the author in October, 1964, and checked again in May, 1965, when it was found no recalibration was necessary. The NRAO position list (Pauliny-Toth, private communication) for the 3C (Bennett 1961) sources was used as the standard. The estimated systematic error in the positions is 2′, somewhat large because the declinations in the observed region are larger than 65° and few radio sources suitable for position calibration exist so close to the celestial pole. The random errors in position are not greater than about 30″.

b) Receiver

The receiver was composed of an Airborne Instruments Laboratory parametric amplifier, a tunnel diode amplifier, and a frequency converter (i.f. ≃ 30 mc) which were mounted at the focus of the telescope, followed by a 100-channel autocorrelation receiver which served as the spectrograph.

The total system noise temperature was 190° K during the first observing period and

220° K during the second. The frequency response of the front end configuration was sufficiently flat over the band width of our profiles so as not to introduce any effects larger than the temperature sensitivity used. The short-term stability of the configuration was very good and gain variations were almost never noticeable in scans up to 6 hours in length.

The autocorrelation receiver has been described by Shalloway (1964). This receiver measures the power spectrum of a signal by measuring its variation with time rather than by measuring the power within wavelength intervals; the complete theory of this type of receiver has been given by Weinreb (1963). The present observations were taken with a total band width of 250 kHz (about 50 km/sec) and were reduced with the "cosine" weighting function which yields an equivalent 50-channel filter receiver. The band pass of each equivalent filter is approximately Gaussian with a half-power band width of 5 kHz, having negative and positive sidelobes of gain less than 4 per cent relative to the gain at its center.

The system was operated in the usual Dicke-switched (Dicke 1946) fashion, being switched to a comparison frequency of about 1423 MHz (−550 km/sec) every $\frac{1}{2}$-sec interval. The equation for the rms noise fluctuation for a perfect system of the present type is (Weinreb 1963)

$$T_{\mathrm{rms}} = \frac{2.41\ T_R}{\sqrt{\tau B}} \tag{4}$$

(about 0.6° for the present observations). Here T_R is the receiver noise temperature, τ is the integration time in seconds, and B is the half-power band width in cycles per second. Observations of globular clusters by Heiles and Henry (1966) and of external galaxies by Morton Roberts (private communication) show that for integrating times of up to at least 10 min this equation is accurate.

The receiver integrates for 10 sec and writes the observed autocorrelation function (equivalent to a complete line profile) and all other relevant data on magnetic tape. This process is automatically repeated every 10 sec. During every other 10-sec interval a noise tube, which is located in the short transmission line connecting the feed to the parametric amplifier, is automatically turned on for those $\frac{1}{2}$-sec intervals during which the receiver is observing the hydrogen frequencies; this provides a continuous measurement of the gain of the system throughout an observation. The noise tube introduces a broad-band signal of equivalent temperature approximately 10° K.

The complex electronic system described above performed superlatively throughout the entire observing period, with the exception of an initial 6 weeks during which several major faults were discovered and corrected. During regular observing the fraction of time lost because of malfunction of any part of the system was about 3 per cent.

c) Temperature Scale

The calibration of the temperature scale of the system could have been carried out in two ways. One way would be to calibrate the system on the basis of other observers' measurements of hydrogen in various parts of the sky. This method is affected by the error beam, as noted above. The other way is to observe small radio sources having well-established intensities. The hydrogen brightness temperature scale then depends on the ratios η_a/η_B and $\eta_a/0.905$[1] and, hence, depends directly on the aperture efficiency. Absolute measurements of aperture efficiency are quite difficult, and a conservative estimate might place the error in the measured value larger than 10 per cent. We feel, however, that the second method is preferable in view of the large contribution of the error beam of the 300-foot antenna.

[1] The aperture efficiency determines the peak antenna temperature produced by a small source. The main beam efficiency determines the antenna temperature produced by a small cloud of hydrogen; the sum of the main beam and the error beam efficiencies, 0.905, determines the antenna temperature produced by a large extent of hydrogen. See the discussion of the antenna above.

The radio sources used for calibration, 3C 348 and 3C 353, were normally observed each day during the two observing periods. The noise-tube intensity was found by comparing the deflection it produced in the total power output of the receiver with that produced by the sources. In deriving the peak antenna temperature due to each source as it drifted through the main beam, the source fluxes listed by Kellermann (1964) were used, proper account being taken of the source sizes as given by Maltby and Moffet (1962). The determinations of the noise-tube intensity from the two sources differed by 3.7 per cent. The daily variation in the determinations was less than ± 2.5 per cent of the mean values for the observing periods, which were the values actually used. At least some of the daily variation was due to real fluctuations in the noise-tube intensity.

Westerhout (private communication), in his survey of the galactic plane with the same equipment and reduction procedures as used here, has noticed day-to-day variations in hydrogen-line antenna temperatures of about 10 per cent. Such variations may also exist in the present data, although they were neither looked for nor noticed. Similar effects have been noticed at the Hat Creek Radio Observatory, and were eventually traced to a time-variable residual gain of the parametric amplifier at the image frequency (H. Weaver, private communication). This is the only reasonable explanation of all those considered for the gain variations observed with the present equipment.

The absolute calibration of the brightness temperature is known only as well as the aperture efficiency, i.e., to about 10 per cent; in addition, the relative calibration of the antenna temperature may fluctuate by 10 per cent if the gain variations noticed by Westerhout appear here also. The absolute calibration of antenna temperature, found from the daily measurements of 3C 348 and 3C 353, is uncertain by 3.7 per cent. Neverthelesss, despite these uncertainties the profiles presented in Figure 2 (see below) agree excellently in all respects with data of other investigators.

d) Observational Procedure

The telescope was left pointed at the same declination for the duration during which data were taken (a "scan"). The beginning and end times of a scan were usually chosen so that the scan began and ended at the boundary of the region defined by $l^{II} \simeq 100°$–$140°$, $b^{II} \simeq 13°$–$17°$. Scans were usually separated by 5′ in declination. Approximately 60 days of observing 8 hours per day were required to cover the area of approximately 160 square degrees. The magnetic tapes on which the receiver wrote all the pertinent data were subsequently read directly into an IBM 7040 computer, with which the positional and velocity information and the line profile were computed and written on another magnetic tape. These reduction programs were written for general use by G. Westerhout and H. Wendlandt.

The information obtained during a scan then consisted of a series of line profiles spaced by 20 sec of time. These were smoothed in the direction of right ascension (α) (the declination remains constant throughout a scan) according to the convolution integral

$$T_a'(\alpha_0) = \frac{3}{4\Delta\alpha} \int_{\alpha_0 - \Delta\alpha}^{\alpha_0 + \Delta\alpha} T_a(\alpha) \left[1 - \left(\frac{\alpha - \alpha_0}{\Delta\alpha}\right)^2\right] d\alpha\,, \tag{5}$$

where $T_{a(\alpha)}$ is the original antenna temperature at frequency f as a function of right ascension, and $\Delta\alpha = 0.565/\cos\delta$ minutes of time. $T_a'(\alpha_0)$ was computed only every 30 sec of time. This interpolation formula, which increases the effective HPBW of the main beam in the direction of right ascension by 20 per cent, provides the necessary continuity between individual data points to make plots of constant temperature versus frequency and right ascension easily and automatically in a computer.

Such plots were made for all scans. The plot for a typical scan is shown in Figure 1. Note that the antenna temperature of the small features is too small relative to that of the large features because the effective beam solid angle efficiency depends on the size

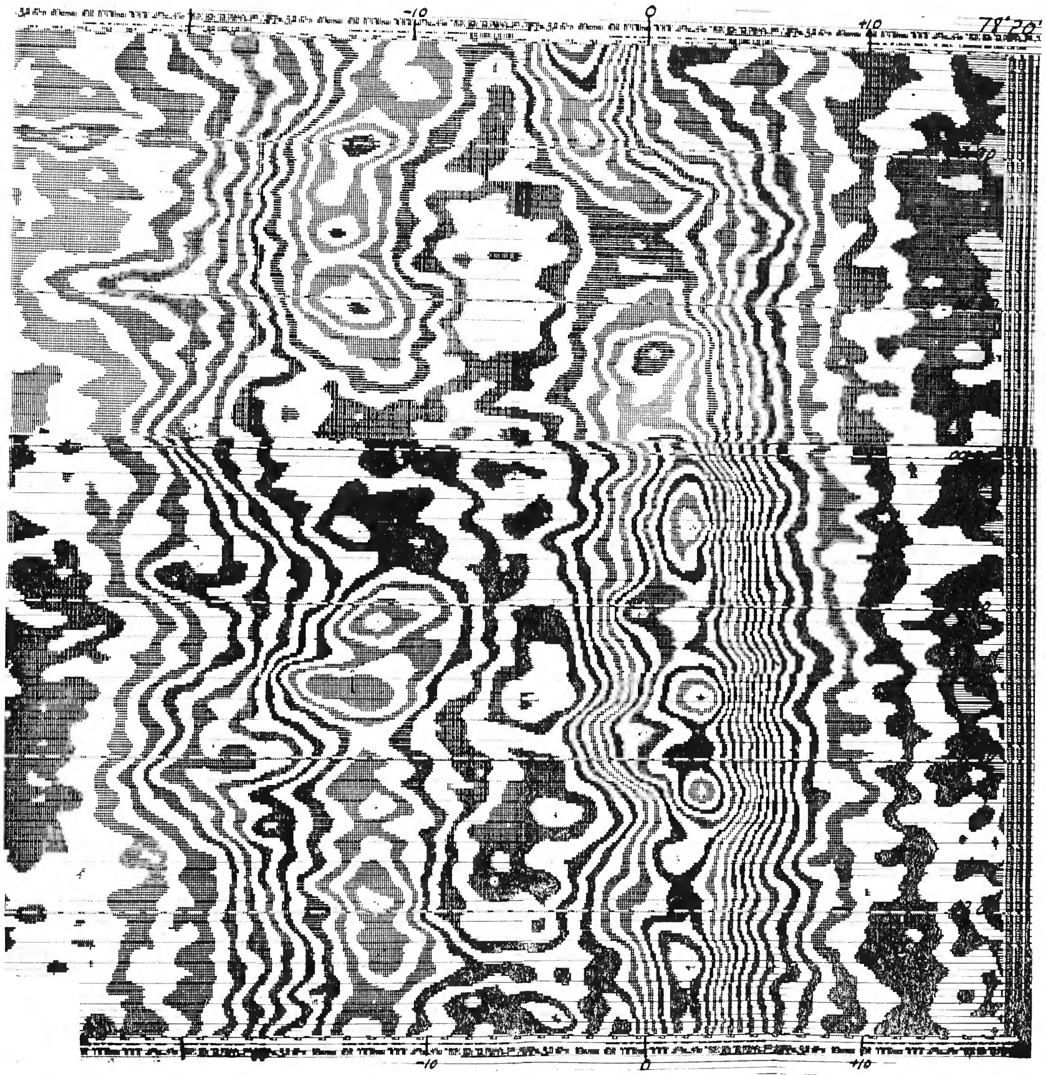

FIG. 1.—Sample of a map of contours of constant antenna temperature versus velocity and right ascension (1950) for a scan in which the declination (1965) remains constant, equal to 78°20′. Velocity (in km/sec) increases to the right; right ascension increases downward. The frequency and velocity scales are with respect to the local standard of rest. The contours are labeled by even numbers, increasing with increasing antenna temperature, alternated with blanks; above the number 8 the contours are labeled with the English alphabet, *A* . . . *Z*, alternated with blanks. Unlabeled maxima and minima are marked with "+" and "−" signs, respectively, to resolve the ambiguity. The zero of the antenna temperature scale, not precisely defined since the total velocity range observed is only about 50 km/sec, is defined approximately by the antenna temperature near +10 km/sec since little hydrogen exists at that velocity in the observed region. The antenna temperature between two successive labeled contour lines is 2.64° K. The total half-power width in frequency is 5 kHz (12 horizontal spaces); in right ascension, 12′ (about 7 lines). This map, originally four computer pages wide, has been greatly reduced in size from the original.

of the object; see the discussion of the antenna above. Most of the plots have been photographed and printed as a catalogue for general distribution by the National Radio Astronomy Observatory (Heiles 1966*a*). This kind of plot was first used, to the author's knowledge, in meteorological applications (see Ulam 1964).

According to equation (5) the effective integrating time, approximately equal to $4\Delta\alpha/3$, increases with increasing declination. This is, in fact, one reason why the present region was chosen, because the longer effective integrating time yields a smaller rms noise temperature, in accord with equation (4). The "contour unit" ($\frac{1}{2}$ the temperature difference between two adjacent dark lines in Fig. 1) was varied with declination in order to take maximum advantage of the sensitivity of the system. In general, the contour unit was chosen equal to $2.82\sqrt{(\cos\delta)}$ °K $\simeq 2.4\ T_{rms}$ (the formula given by Heiles 1966*a*, *b*, slightly different from this, is incorrect).

The epoch of the equatorial coordinates throughout this work is 1950 for right ascension, 1965 for declination; this unusual combination was chosen because the 1965 declination remains absolutely constant during a scan, while 1950 coordinates are more useful for comparison with other work. The 1950 declinations can be found to within 2′ in the region by subtracting 3′ from the 1965 declinations. The relationship of galactic coordinates to equatorial coordinates in the region can be seen in Figure 3; the galactic coordinates are expressed in the new system (Blaauw, Gum, Pawsey, and Westerhout 1959) unless otherwise indicated. Velocities are always given relative to the local standard of rest as defined by the average interstellar medium, the same standard used by van de Hulst *et al.* (1954).

e) Comparison of Present Data with WTB's Profiles

It is useful to compare some of the present results with those obtained by WTB, who have made the most complete and accurate intermediate latitude general survey to date. In Figure 2 parts of five profiles obtained by WTB are compared with those of the

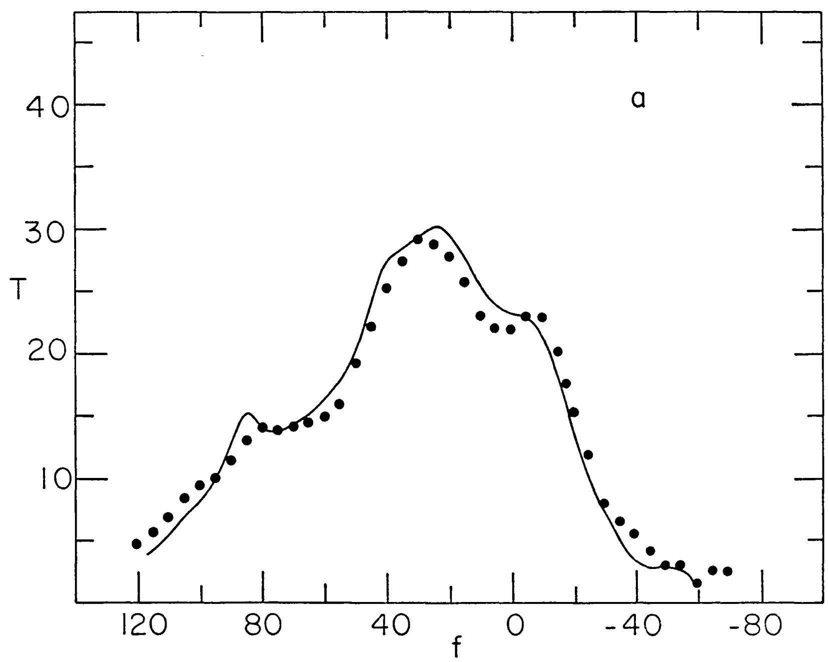

FIG. 2.—Comparison of the present data with profiles by WTB; brightness temperature T_b versus frequency f. The zeros of the profiles from the present data have been adjusted to equal those of WTB near $f = -50$ kHz; the beam efficiency used was 0.905. The solid line represents the present observations (from T_a'); the open circles, smoothed 300′ profiles (from T_a''); the filled circles, WTB profiles. For all profiles $b = 15°$. For *a*, $l^{II} = 70°$; *b*, $l^{II} = 80°$; *c*, $l^{II} = 90°$; *d*, $l^{II} = 100°$; and *e*, $l^{II} = 110°$.

1967ApJS...15...97H

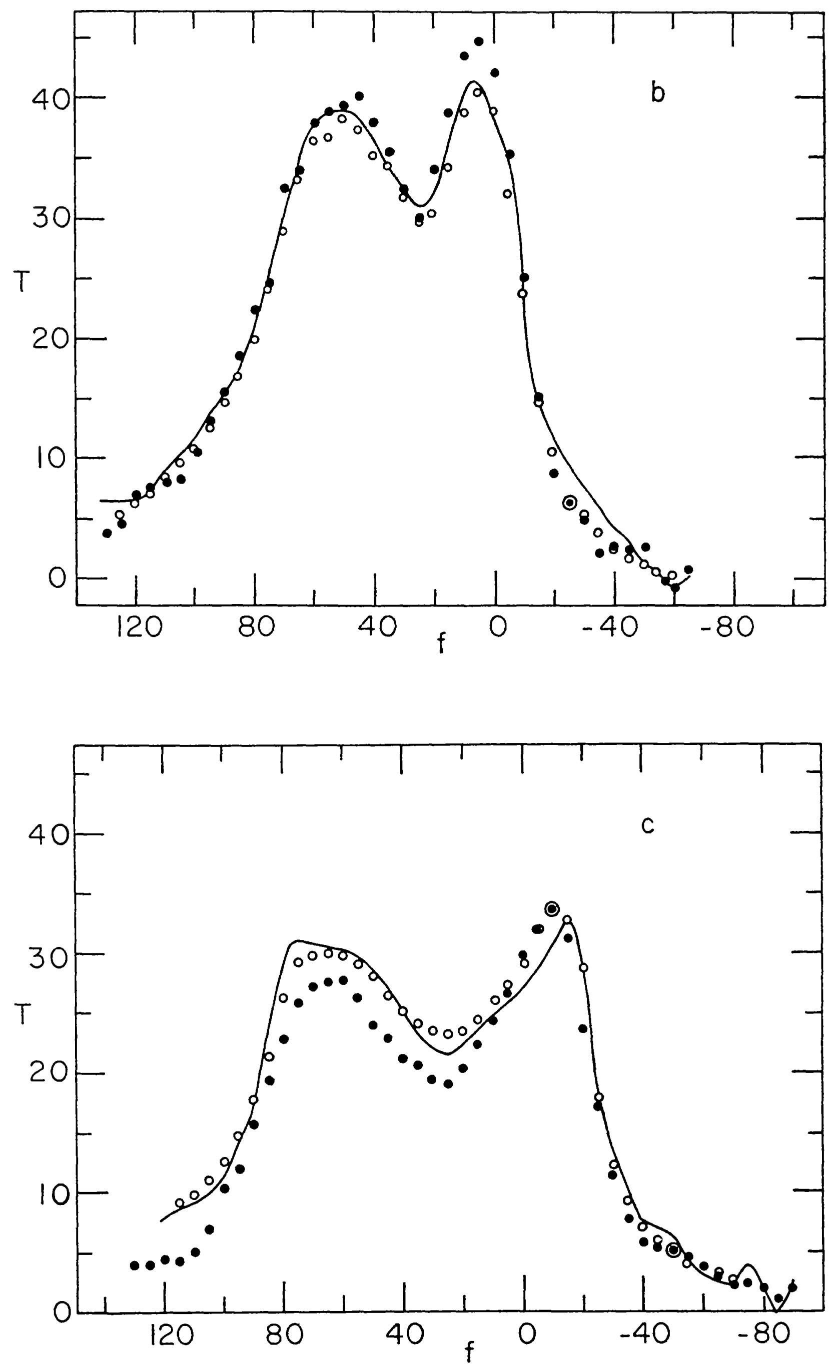

FIG. 2.—*Continued*

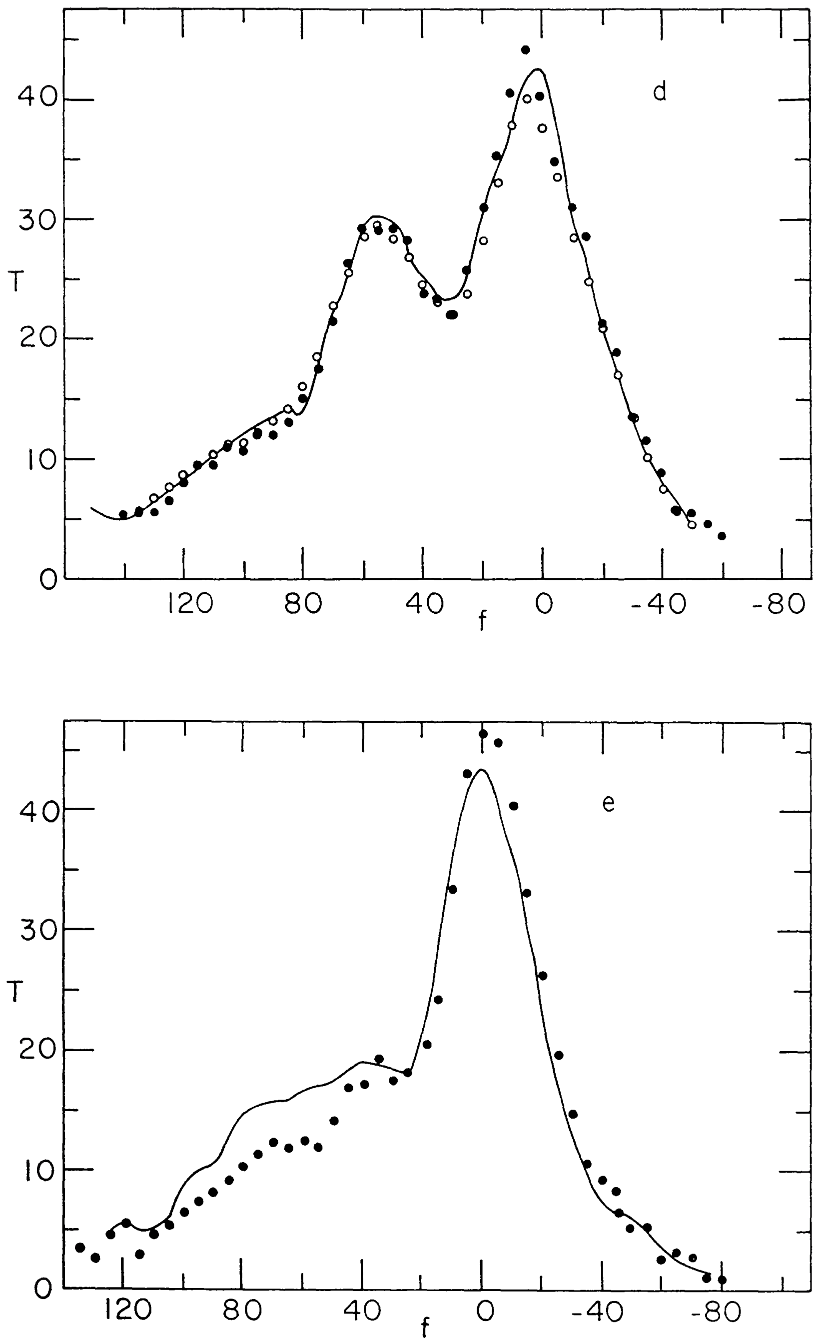

FIG. 2.—*Continued*

present work. The WTB survey was performed with a frequency resolution of 10 kc and a HPBW of 33'.5. Our data for profiles at $l^{I} = 90°$ and 100° were taken during the first observing period; the data for the other profiles in Figure 2 were obtained during the second period. The zero of our temperature scale, not precisely defined because the total velocity range observed is only 50 km/sec, was adjusted by equalizing the two brightness temperatures near the velocity of +10 km/sec because WTB's data indicate that little hydrogen exists at this velocity in this region. The difference in beam width was accounted for in three of the profiles by evaluating approximately the convolution integral

$$T_a''(\theta_0,\phi_0) = \int\int T_a'(\theta,\phi) f(\theta-\theta_0,\phi-\phi_0) d\theta d\phi \,, \tag{6}$$

where

$$f(\theta,\phi) = \begin{cases} \frac{1}{400\pi}, & (\theta^2+\phi^2)^{1/2} < 20' \\ 0, \text{ otherwise} \end{cases} .$$

Here the angles θ and ϕ are expressed in minutes of arc, and T_a' is defined by equation (5). The brightness temperatures, obtained from T_a'' with $\eta = 0.905$ in equation (3), are plotted in Figures 2*b*, 2*c*, and 2*d*.

The general agreement of the two sets of profiles is very good. The effects of smoothing by the wider beam are immediately apparent. The surprising features, such as the differences between some of the WTB profiles and the smoothed 300-foot antenna profiles, and the narrower components in these profiles relative to the unsmoothed 300-foot antenna data, can be qualitatively accounted for by taking into consideration the neighboring hydrogen structure and the influence of the error beam of the 300-foot antenna.

The contour maps for scans over the same positions, taken in the two observing periods, differed insignificantly.

III. PRELIMINARIES

a) The General Features of the Region

The observed region is shown in Figure 3 and lies between the galactic plane and the north celestial pole. A large part of the region coincides with a tongue protruding up from the zone of avoidance denoted by Hubble (1934) as the "Cepheus flare," which extends approximately from longitude (new system) 100°–120°. WTB noticed that the region has unusually pronounced double-peaked hydrogen line profiles; Davies (1960) has shown that the variation of hydrogen with galactic latitude for longitudes in the region is unusual. The region lies outside of Gould's belt.

Lodén (1961), in his stellar polarization survey for some of Kapteyn's Selected Areas, found polarizations of up to 4 per cent and extinctions of up to 2.4 mag in Selected Area 2 ($l^{II} = 120.4°$, $b^{II} = 13.2°$) which lies in the Cepheus flare, and polarizations of up to 2.5 per cent and extinctions of up to 1.2 mag in Selected Area 3 ($l^{II} = 135.1°$, $b^{II} = 17.6°$) which lies outside of the flare; the mean values of polarization and extinction are $\frac{1}{3}$ the maximum values. Seeger, Westerhout, Conway, and Hoekema (1965), in their 75-cm radio continuum map of the sky, show that the radio emission in the region appears normal but rises several degrees in galactic longitude off both ends of the region. The survey of radio polarization by Berkhuijsen and Brouw (1963) at 75-cm wavelength shows anomalously high polarization as compared to that elsewhere near latitude 15°, particularly near the high-longitude end of the region where the nearby polarization is larger than anywhere else in the whole sky. The comparison of this survey with that of Berkhuijsen, Brouw, Muller, and Tinbergen (1964) at 50 cm shows that Faraday rotation is present throughout the region; as quoted by these authors, a typical rotation measure $n_e BL \simeq 0.5 \times 10^{-5}$ gauss pc^{-1} cm^{-3}. These data taken together show that a

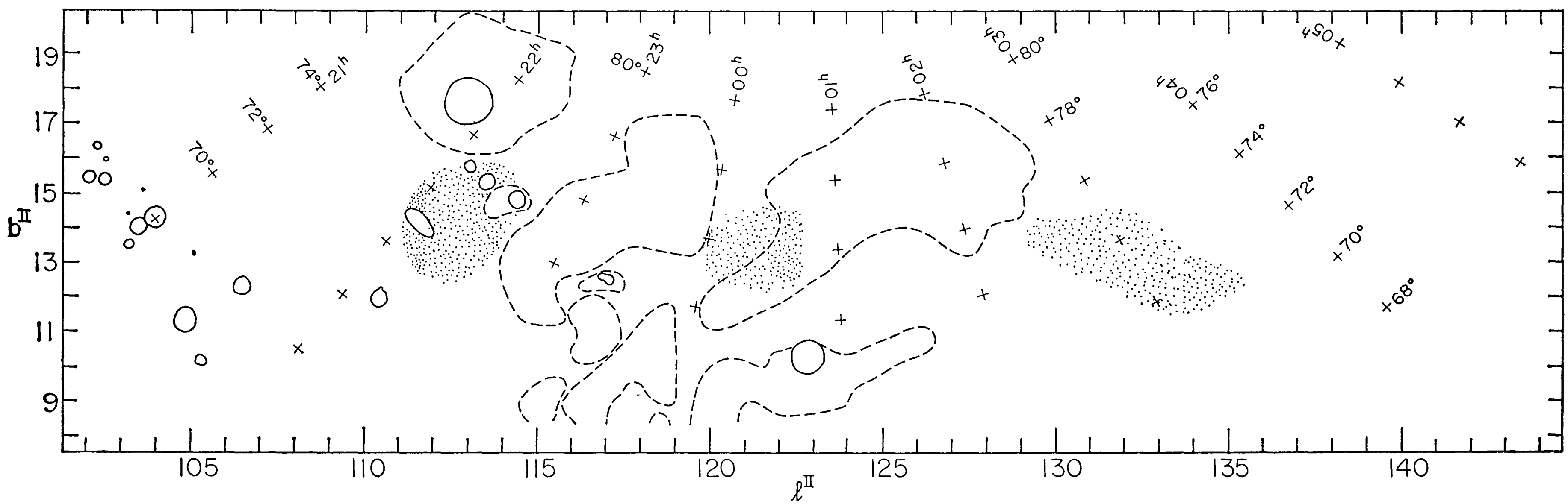

FIG. 3.—Space distribution of optical features in and around the region. The objects denoted with a solid line are Lynds's clouds; those by a dashed line are Khavtassi's clouds. The objects formed by many dots are regions found on the Palomar prints which present a vague dusty appearance. The equatorial coordinate system is indicated on the map.

magnetic field exists somewhere along the line of sight; the existence of optical polarization indicates that the field is probably associated with the interstellar gas, since the gas is probably associated with the grains. Both the optical and radio data indicate that in and around the present region the field is usually, but not always, parallel to the galactic plane.

Very few conspicuous optical features appear in or near the region. Three diffuse galactic nebulae were catalogued by Cederblad (1946). The author found two faint reflection nebulae near the stars HD 210806 and HD 211319 on the Palomar prints. Some dust clouds exist in the region; Khavtassi (1960) indicates several very large, weak dust clouds scattered throughout, Lynds (1962) indicates several smaller, more opaque dust clouds, and the author examined the Palomar prints and found regions which present a vague impression of being obscured by dust. The locations of these objects are indicated on Figure 3. All of the nebulae and most of Lynds's clouds occur near the low-longitude end of the region, i.e., in the middle of the Cepheus flare.

b) Adoption of a Distance to the Hydrogen

The distance to the observed hydrogen can be estimated in three ways: (1) The hydrogen is expected to be associated with dust clouds and diffuse nebulae, to which the distances can be obtained from optical methods. (2) The distance to the hydrogen can be inferred from its distribution with galactic latitude. (3) The distance can be found if we assume that the velocity of the hydrogen is caused by pure differential galactic rotation.

We first consider the optical methods. The spectroscopic parallaxes of the exciting stars of the nebulae mentioned above have been obtained using the magnitudes and classifications in the *HD* catalogue, assuming that the stars lie on the main sequence as defined by Keenan (1963) and that 0.25 mag of optical extinction is present. The average of these distances of the five stars is 390 $\pm$ 27 (p.e.) parsecs. Distances can also be obtained from star counts in and around dark clouds; Bok (1937) quotes 500 parsecs for a dust cloud near the region. Elvius (1956) has measured color excesses of stars in many of Kapteyn's Selected Areas. In Selected Area 3 he finds that the absorbing material lies in two regions along the line of sight, distance 275 and 500 parsecs, which have extinctions of about 0.1 and 0.6 mag, respectively. In Selected Area 2 he finds that the dust is concentrated near 525 parsecs distance and produces an extinction of 1.2 mag. In Selected Areas near the present region, Nos. 7 (l = 108.5, b = 20.8) and 18 (l = 100.3, b = 7.1), the material also lies in two regions, distant about 300 and 700 parsecs; the extinction of the nearer material is 1.2 mag., and that of the more distant material is 0.4 and 2.7 mag., respectively. Lodén's polarization data for these four regions agree well for the distance of the nearby material in all of the areas but No. 2; his distance determinations of the more distant material do not agree well with the results of Elvius.

The second distance estimate is based on the latitude dependence of the projected hydrogen density. The average distribution of hydrogen with distance, z, from the galactic plane is a bell-shaped curve. The total half-width of the distribution is 220 parsecs (Schmidt 1957). The recent increase of the galactic distance scale by 20 per cent, while increasing this value, is probably offset by Schmidt's overestimation of the half-width from using an antenna and receiver of insufficient resolution (Kerr, private communication). This distribution with z can be converted to a distribution of hydrogen with distance along the line of sight when one observes hydrogen at $b \neq 0°$; the most probable distance which results when observing at a latitude 15° is about 1000 parsecs. However, Schmidt's distribution law is only valid on the average; variations are to be expected (Kerr and Westerhout 1965). One indication of departure from the idealized distribution is the projected hydrogen, N_H, not varying as $1/\sin b$; it does for most intermediate latitude hydrogen (McGee and Murray 1961). Two supplementary sets of observation indicate that such a departure does exist in the present region. These con-

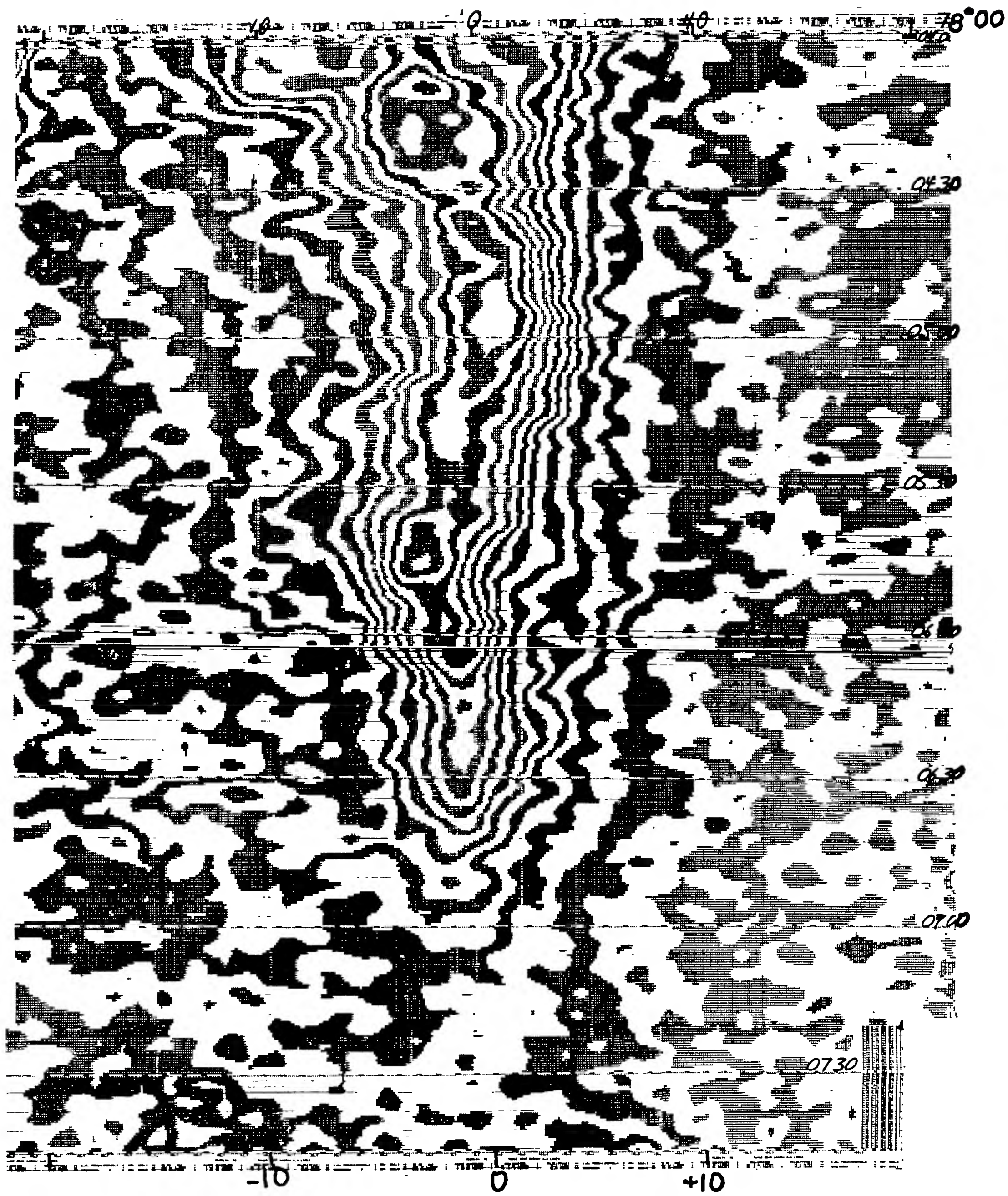

(*a*)

FIG. 4.—Contour maps of constant antenna temperature versus right ascension and velocity for a set of auxiliary scans, which were taken all the way around the celestial pole at declination about 79°; this corresponds roughly to a circle in galactic coordinates of radius 11° centered near longitude 123°, latitude 27°. The contour interval (half the temperature difference between two black lines) is approximately 1°.4. No hydrogen appears in the intervals of right ascension not shown here except a small cloud near right ascension 11^h00^m, part of which is visible on Fig. 4*b*. In Fig. 4*a* the galactic latitude increases continuously with right ascension; in Fig. 4*c* it decreases. See the caption of Fig. 1.

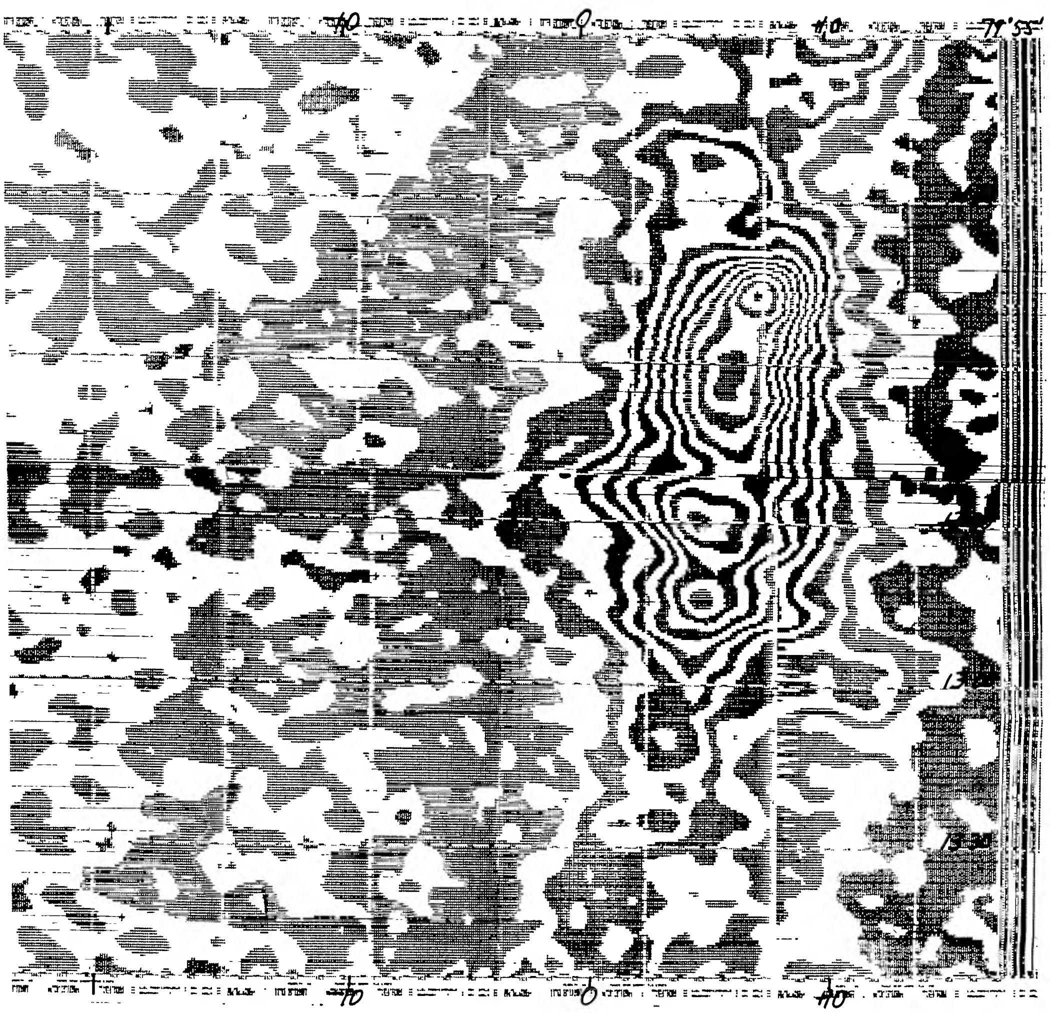

(*b*)

FIG. 4.—*Continued*

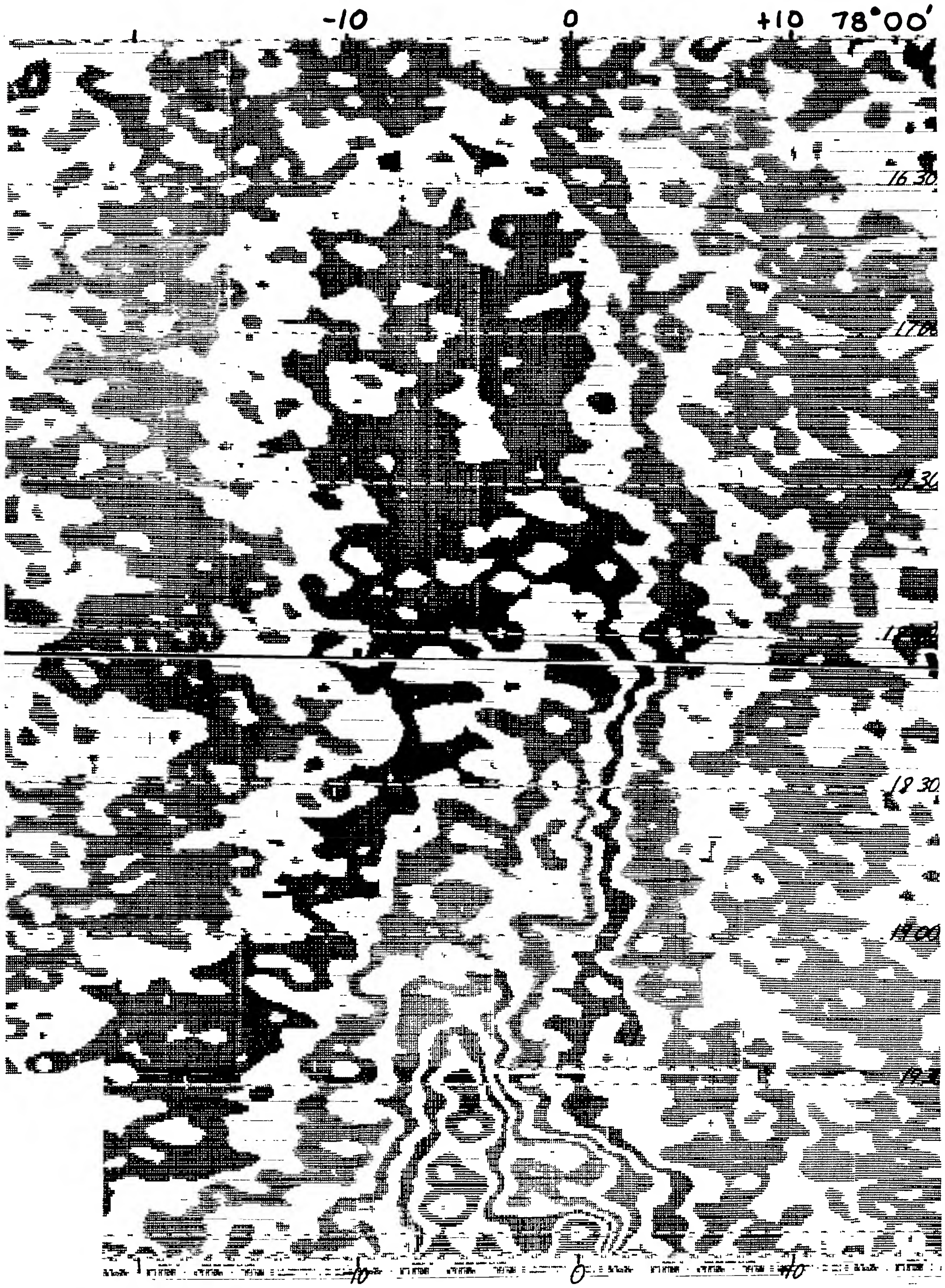

(*c*)

FIG. 4.—*Continued*

firm the more extensive observations by Davies (1960) and Erickson and Helfer (1960), whose data in addition indicate that the apparent deficiency of hydrogen at the higher latitudes is matched by an excess of hydrogen at the intermediate latitudes, relative to other longitude regions.

This behavior is revealed by contour maps of antenna temperature versus velocity and galactic latitude, for constant longitude, which were made using data from an auxiliary set of observations which extends the latitude range covered by this survey for a modest longitude interval (see Heiles 1966*b*). These auxiliary observations consist of scans separated by 1° in declination, several hours long, centered on right ascension 00^h50^m (cf. Fig. 3). These observations extend the total declination range covered to 71°–83° near galactic longitude 123°; this corresponds to a range in latitude of about 8°–20°.

The total longitude range over which these auxiliary data are complete, about 10°, is insufficient to derive the typical functional dependence of N_H on b. However, it is sufficient to show that N_H decreases more rapidly than $1/\sin b$, and in addition that the velocity of the gas does not vary systematically with increasing latitude.

At a certain latitude the decrease of N_H is extremely rapid, almost discontinuous; this was discovered in another set of supplementary scans taken at declination 78° or 80° which were continued all the way around the celestial pole. In galactic coordinates this corresponds roughly to a circle of radius 11° with its center near $l = 123°$, $b = 27°$. Some of the resulting contour plots are shown in Figure 4. Figure 4*a*, a scan in which the galactic latitude continuously increases with increasing right ascension, shows an abrupt decrease in the amount of hydrogen near right ascension 06^h45^m ($l = 116.5°$, $b = 27°$). Aside from an isolated hydrogen cloud near right ascension 12^h00^m shown in Figure 4*b* (see § V*h*), the amount of hydrogen remains almost zero until an abrupt increase occurs in the amount of hydrogen near 19^h15^m ($l = 109.6°$, $b = 26°$), seen in Figure 4*c* in which the galactic latitude continuously decreases with increasing right ascension. Further data near 11^h, not shown here, confirm the absence of hydrogen with velocity from −75 to +35 km/sec.

Interstellar matter is stratified in plane-parallel layers, on a galactic scale. However, the excessively rapid decrease of hydrogen with increasing latitude implies that the observed hydrogen, including the background component, is not so distributed. A spatial distribution which does produce these observational results is one having little hydrogen near or above the Sun; if this is the true distribution, the observed hydrogen cannot be in the immediate vicinity of the Sun.

The latitude independence of the velocity of the gas implies that velocity cannot be used as a distance indicator. An estimate of its distance can be obtained from the abrupt decrease in hydrogen in Figures 4*a* and 4*c*. This decrease probably represents the "top" of the hydrogen z distribution; if it occurs at $z > 110$ parsecs, the gas of the LVS (low-velocity sheet) must be at least 250 parsecs distant since the associated galactic latitude is 27°.

The third distance estimate is based on the velocity of the gas. The apparent lack of correlation of velocity with galactic latitude mentioned above indicates that the observed velocity is probably not entirely due to differential galactic rotation because the mean distance to the hydrogen increases with decreasing latitude if the hydrogen is ideally distributed. However, because the WTB profiles do indicate that the velocity of intermediate-latitude hydrogen is usually influenced by differential galactic rotation (see Takakubo 1963; Blaauw, 1962) we can obtain a crude distance estimate by using the assumption that the theory of differential galactic rotation is strictly applicable. The −12 km/sec velocity of the high-velocity peak of the hydrogen profiles near longitude 135° (Fig. 5) then implies a distance of 800 parsecs if we use the Oort constants given by Schmidt (1965). We shall argue below that the gas in the low-velocity peak cannot be too distant from the gas in the high-velocity peak, and thus is not in the im-

1967ApJS...15...97H

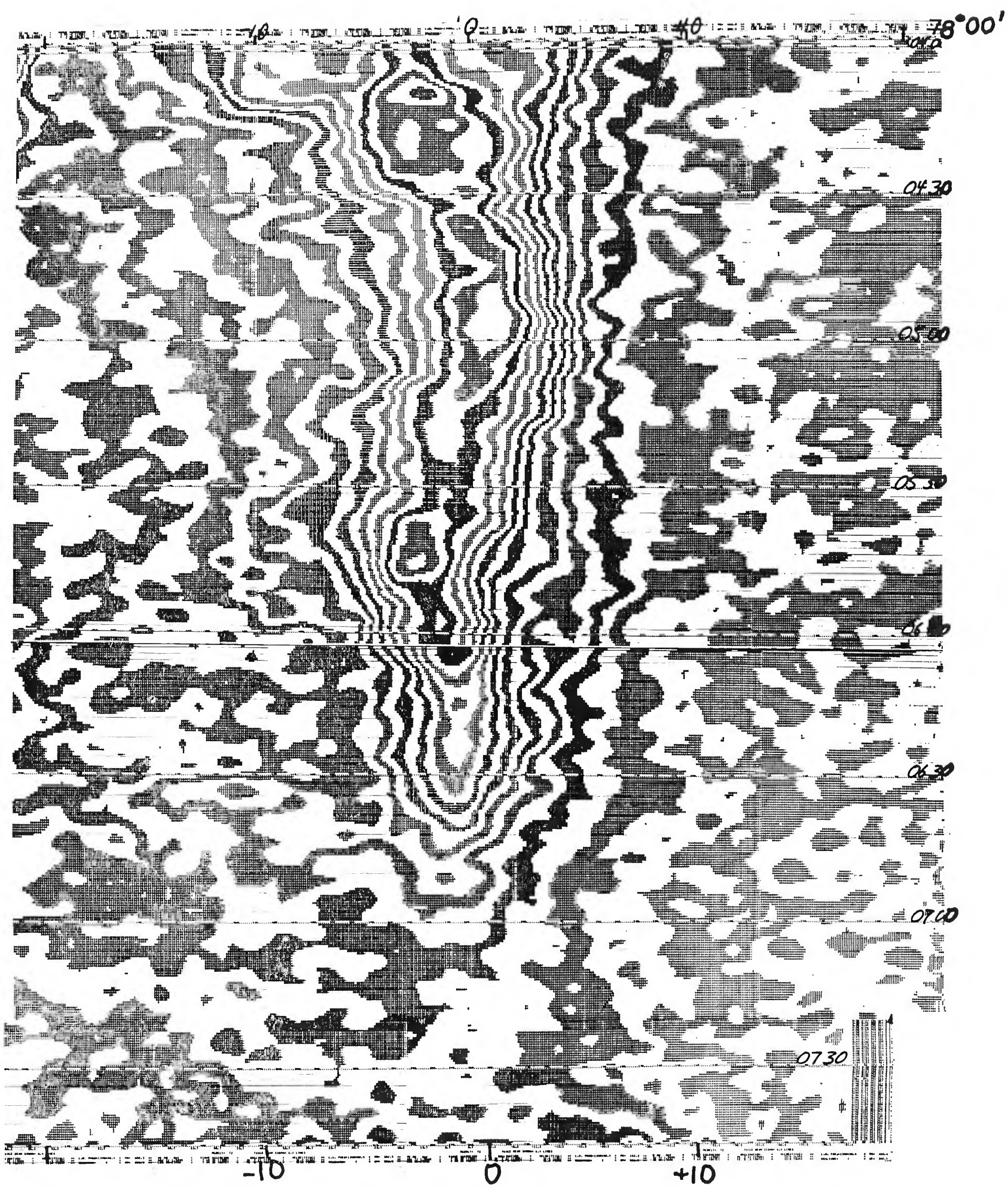

(*a*)

FIG. 4.—Contour maps of constant antenna temperature versus right ascension and velocity for a set of auxiliary scans, which were taken all the way around the celestial pole at declination about 79°; this corresponds roughly to a circle in galactic coordinates of radius 11° centered near longitude 123°, latitude 27°. The contour interval (half the temperature difference between two black lines) is approximately 1°.4. No hydrogen appears in the intervals of right ascension not shown here except a small cloud near right ascension 11^h00^m, part of which is visible on Fig. 4*b*. In Fig. 4*a* the galactic latitude increases continuously with right ascension; in Fig. 4*c* it decreases. See the caption of Fig. 1.

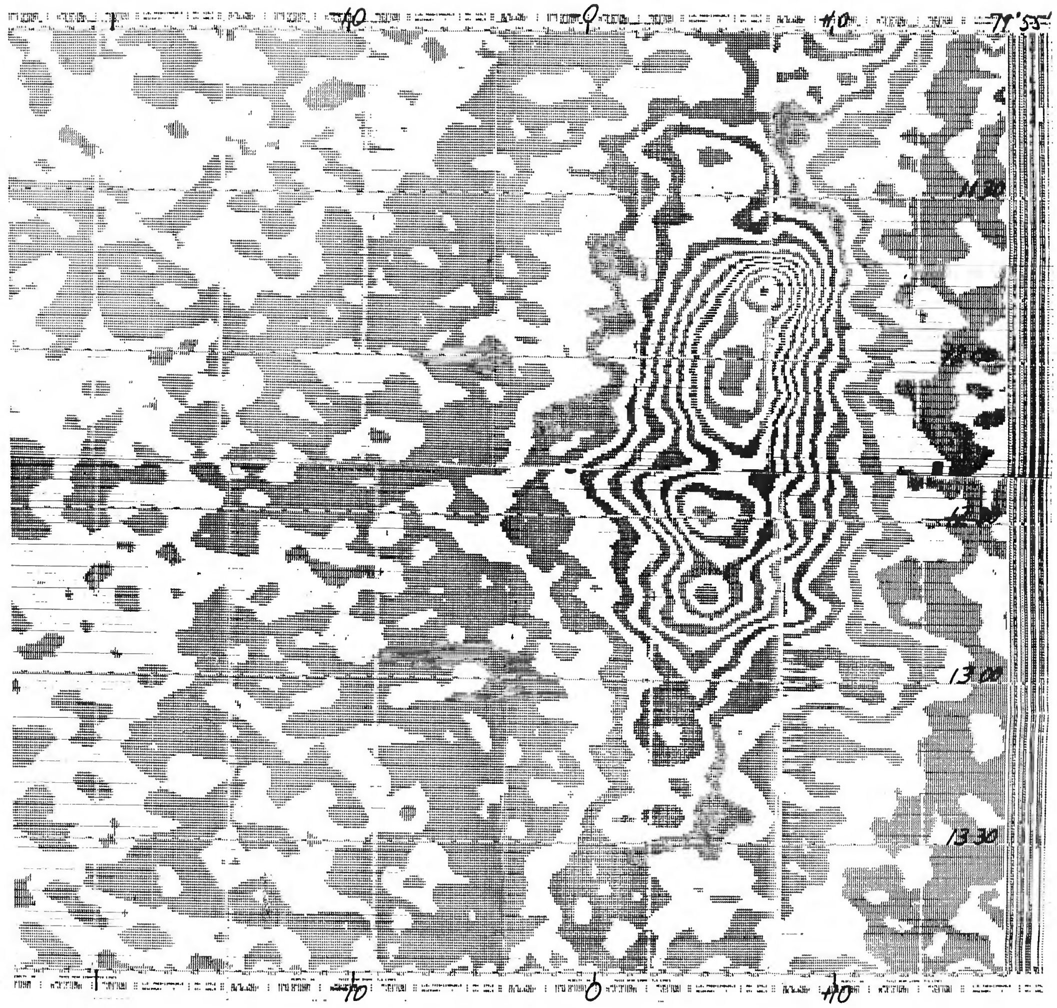

(*b*)

FIG. 4.—*Continued*

(*c*)

FIG. 4.—*Continued*

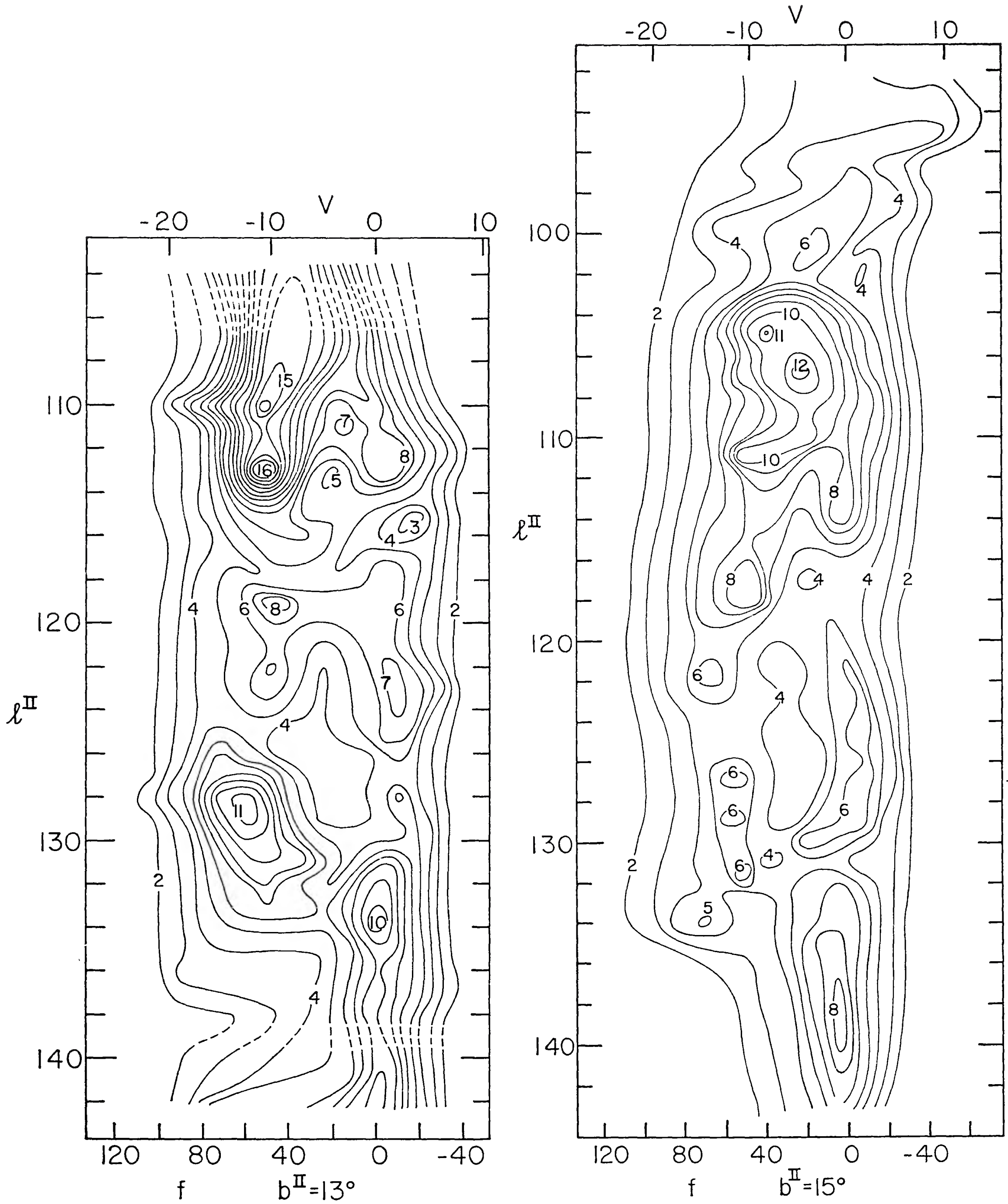

(*a*) (*b*)

FIG. 5.—Contours of constant antenna temperature versus galactic longitude for three galactic latitudes. The interval between contours is 5°; the lowest contour corresponds to $T = 10°$ K. The velocity scale (v) is in km/sec; the frequency scale (f) is in kHz. The data for $l < 104°$ in Fig. 5b were taken from WTB and have $b \simeq 15.3°$ instead of $b = 15°$; the sudden change near $l = 102°$ is real.

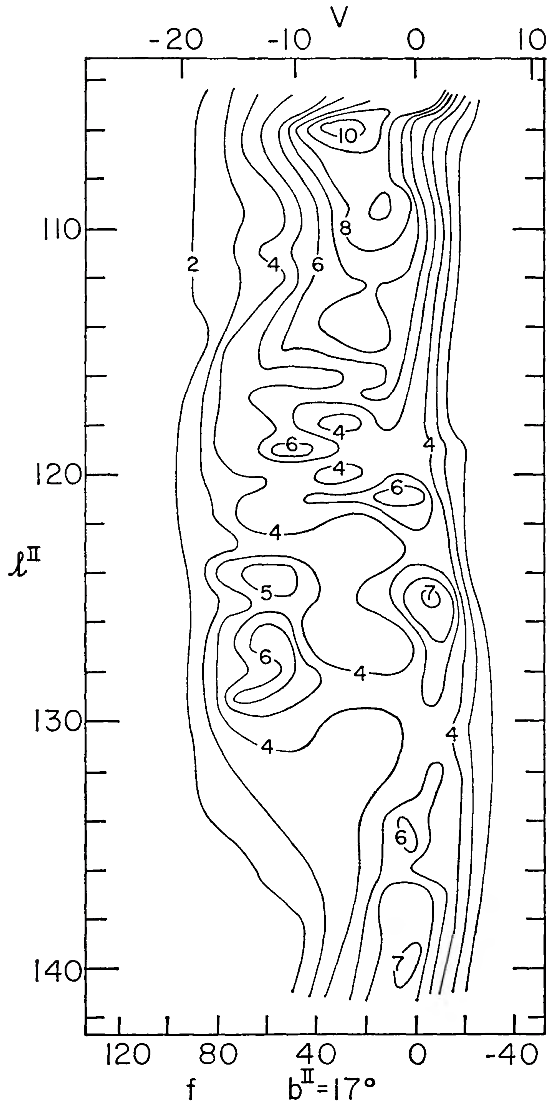

(c)

FIG. 5.—*Continued*

mediate vicinity of the Sun even though it has zero velocity; this point is tentatively confirmed by the lack of interstellar Ca II lines in high-dispersion plates of nearby stars obtained recently by the author.

These methods indicate that the distance to all of the hydrogen lies between 250 and 1000 parsecs; the optical work indicates that the hydrogen is concentrated in two distance ranges along the line of sight. For purposes of conversion of subtended angle to length we shall hereafter assume that the distance to all of the hydrogen observed is 500 parsecs. For purposes of discussion of the geometry of the observed gas, however, we shall assume that the indications of the optical work are correct, i.e., that the gas resides in two concentrations distant about 300 and 500 parsecs throughout most of the region. Unfortunately, the Selected Areas lie outside places where both sheets exist in the line of sight; it is unfortunate that more extensive optical data, referring to other areas within the present region, are unavailable.

IV. CORRESPONDENCE WITH THE STANDARD CLOUD MODEL

The "standard cloud model" (see the summary by Spitzer 1967) is an attempt to describe the essentials of the structure of the interstellar medium in terms of a simple concept and in terms of a small number of parameters. The concept is that nearly all of the interestellar gas is concentrated into self-contained roughly spherical clouds which move independently and suffer elastic or inelastic collisions, possibly sometimes fragmenting. The situation would be somewhat analogous to many sticky, brittle billiard balls rolling on a bounded table. The parameters needed to quantify the concept are simply the average radius and mass of the clouds, and the number of clouds per unit volume in space. Exact values are unimportant. A typical cloud contains perhaps several hundred solar masses and has a radius of several parsecs. About ten clouds per kiloparsec exist in the line of sight, and they move with one-dimensional random velocities of roughly 10 km/sec, so that collision times are about 10^7 years. The internal velocity widths are about 5 km/sec (Spitzer and Skumanich 1952). This model is eminently compatible with all existing observational data.

A primary question is whether or not the model is consistent with the present data. One can show that Schmidt's result implies that the amount of hydrogen in our line of sight, observing at latitude 15°, is equivalent to that in a line of sight in the galactic plane of length about 500 parsecs; thus we should expect to see, at any point, about five clouds in the line of sight. Furthermore, the parameters of the standard cloud imply that each should produce a substantial antenna temperature (say, six labeled contour lines on Fig. 1) and should be about 30 min of time in diameter (using the distance found above). The velocities of the five hypothetical clouds should be randomly spread between about zero and -20 km/sec (partly from differential galactic rotation).

But even cursory examination of Figure 1 shows a completely different appearance. We see instead that the hydrogen is concentrated into two velocity peaks and that the velocities of the peaks are highly systematic over the whole length of the scan. Although some structure exists within each velocity peak, it is hardly large enough to be caused by standard interstellar clouds. No structure or excess hydrogen ever appears in the velocity range -2 to -10 km/sec. Figure 5, which covers the whole length of the observed region, shows the same general picture.

We shall see below that some objects we might wish to call clouds do exist in the region. About ten of these objects were found; the standard cloud model predicts that several hundred clouds should have been found; hence the existence of these few objects is no confirmation of the standard cloud model. This is especially the case since the objects found tend to cluster into groups or have parameters quite different from the standard cloud.

To summarize, the *qualitative* picture which results from the present observations is totally different from the standard cloud model to which the reader has been exposed for many years.

V. THE MAIN OBSERVATIONS

The integral under a typical profile indicates that there are about 10^{21} hydrogen atoms/cm^2 in the line of sight. This is roughly the amount of gas expected from the equivalent length of the line of sight in the galactic plane if the gas were distributed according to Schmidt's relation. The results of Elvius (see § III*b*) concerning typical optical depths due to dust in the region indicate that the mass ratio of dust to gas is roughly $\frac{1}{100}$. The value of this ratio has consequences relevant to the existence of molecular hydrogen which are discussed below (§ V*f*). This value is similar to that found by Lilley (1955) and is typical for the general interstellar medium (Davies 1960; McGee, Murray, and Milton 1963; Heiles 1967).

The over-all distribution of hydrogen with position and velocity can be separated into three components: a background component, which alone produces a profile changing slowly with position and having a large velocity dispersion, and two "velocity peaks." These two velocity peaks characterize most of the line profiles of the region. Within these peaks appear smaller structures which can be characterized by closed three-dimensional objects; large concentrations; and cloudlets, small objects of near-stellar mass. Below, we argue that the gas at each velocity peak resides in a sheetlike structure. Accordingly, we shall hereafter denote the gas in the high-velocity peak by "HVS" (high-velocity sheet) and that in the low, near-zero, velocity peak by "LVS" (low-velocity sheet); these sheets are probably at different distances, the distances of the dust (§ III).

Figure 5 shows approximate contour maps of antenna temperature as a function of velocity and galactic longitude for three latitudes in the observed region. The velocity peaks stretch throughout most of the region, except they merge near $l = 109°$ and then disappear near $l = 103°$, and the HVS disappears (i.e., neither merges nor affects the LVS) near $l = 137°$. The remainder of the hydrogen, which varies slowly with position except near $l = 137°$, comprises the background component. If we imagine all of this gas to be at the same distance, 50 to 75 per cent of the mass is contributed by the background component; the remainder is contributed by the sheets. About 18 per cent of the gas in the sheets is in the form of cloudlets. (See below for descriptions of these structures.)

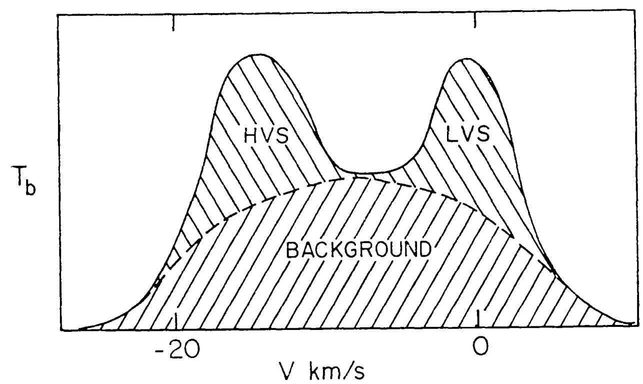

FIG. 6.—A schematic picture of the method used to separate the gas into the three components; the areas comprising the LVS and the HVS are mapped in Fig. 7.

The obviousness of the two-component structure of the profiles permits the making of contour maps of the structure of each component as a function of position, in the approximate manner explained in Figure 6. Such maps are shown in Figure 7. The placement of the contour lines is only approximate, mainly because the zero of the scale is ill defined owing to variations in the amplitude of the background. However, the small wiggles in the contour lines are real and are caused by cloudlets. At the low-longitude end of these maps the contribution from the intermediate-velocity feature produced by the merging of the two velocity components is shown on both maps since it apparently belongs to both of the components together; in part of this region the HVS merges suddenly (in about 20′), resulting in a very large velocity gradient with position and in very striking structures on the contour maps of original data.

Figure 7 presents the general impression that the large-scale structure of the hydrogen is significant. One large, weak feature of each velocity component, concentrations 8 and 9 (in Table 1), is oriented so that its short dimension is parallel to lines of constant galactic longitude. Two narrow rifts, which are characterized by an *absence* of hydrogen, run across the maps near $l = 124°$ for the HVS and near $l = 118°$ for the LVS. The structure in the HVS appears more patchy than that in the LVS; two "cloud groups" (see § V*d* below) occur in the HVS near $l = 112°$, $b = 14°$ and near $l = 128°$, $b = 13°$.

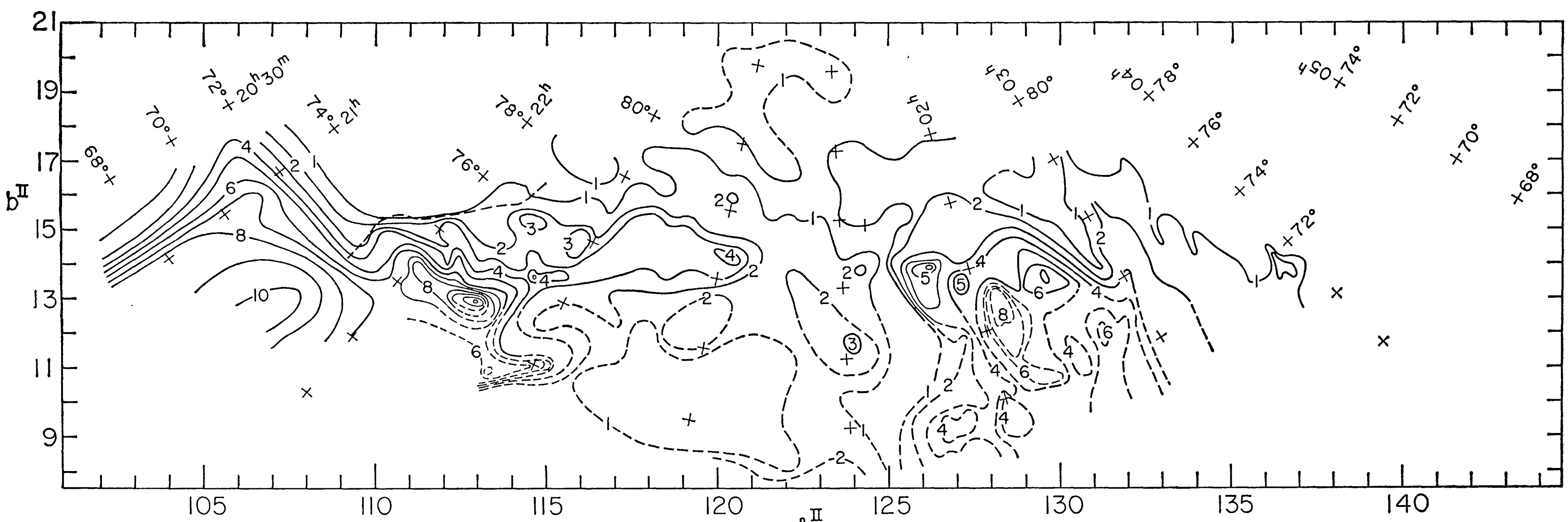

(*a*)

FIG. 7.—Contour maps of number of hydrogen atoms per square centimeter in the line of sight (N_H), versus galactic longitude and latitude, for the two velocity peaks. Fig. 7*a* is for the HVS; Fig. 7*b*, for the LVS. To the left of the thick dashed line in Fig. 7*a* the velocity components merge, so the total excess number of atoms over the background is plotted on both maps. Only the region bounded approximately by $l \simeq 100°$ to $140°$, $b = 13°$ to $17°$, in which the contour lines are solid, was well observed (i.e., covered with scans usually separated by 5′ in declination); the remaining dashed contours were drawn from scans taken every degree in declination (i.e., at declinations 71°, 72°, etc.). The contour interval corresponds to $N_H \simeq 6 \times 10^{19}$ hydrogen atoms/cm². The equatorial coordinate system is indicated on the maps.

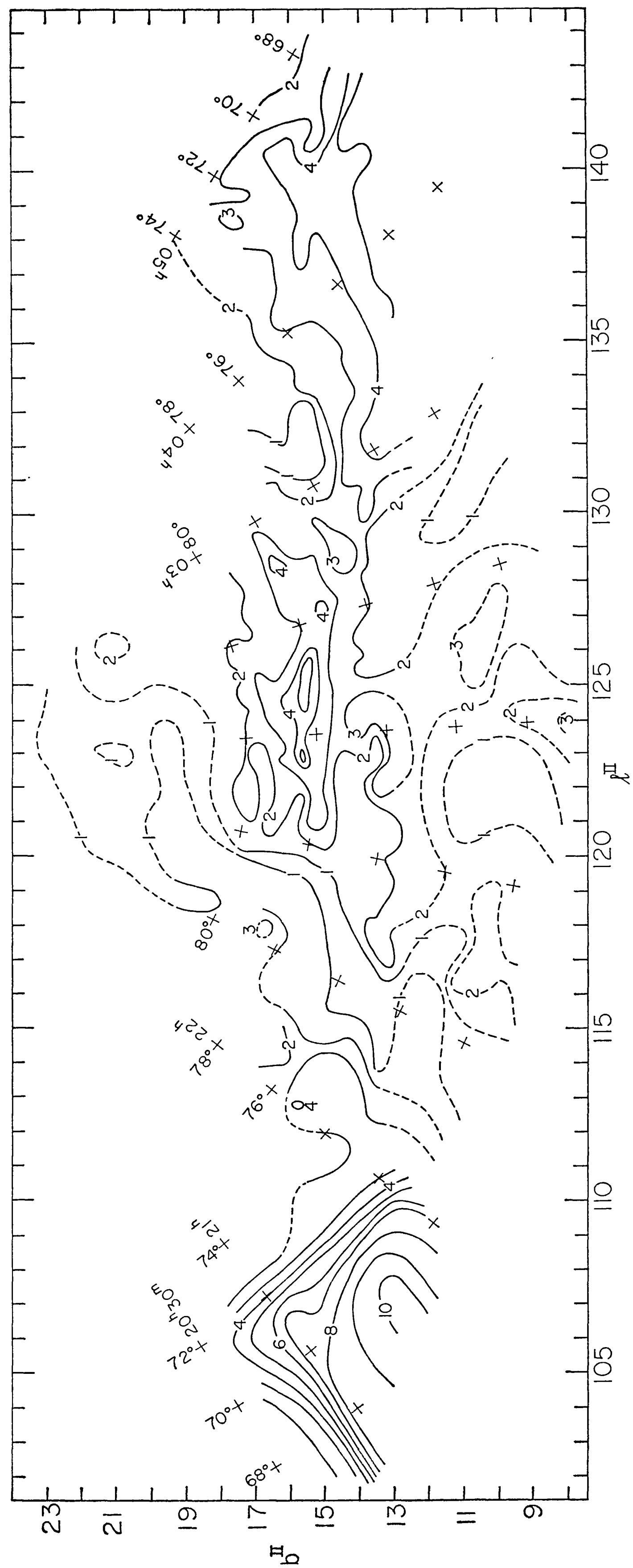

(b)

FIG. 7.—*Continued*

There is some suggestion that the values of N_H for the two velocity sheets are negatively correlated when considered as a function of position; for example, at the positions of the two concentrations in the HVS at $l = 119.0°$, $b = 14.5°$ (concentration 8) and at $l = 128°$, $b = 12°$ (a cloud group) appear weak deficiencies in the LVS. However, this tendency is hardly striking or general.

We now discuss these structures roughly in order of decreasing scale size.

a) The Rifts and the Sheets

We attach particular importance to the establishment of the existence of the rifts; apparently these linear structures are of a new class not heretofore observed. These structures are quite well defined: the boundaries are sharp relative to the width, and the boundaries on the two sides of the rift in the HVS especially follow each other startlingly well. These rifts are easily visible in the original data on Figure 1 near right ascensions 00^h30^m and 22^h50^m for the high- and low-velocity sheets, respectively.

From geometrical considerations it is very improbable to see a linear rift in the interstellar gas, unless the thickness of the gas in the direction of the line of sight is comparable to the width of the rift. Because the rifts can be followed over such large distances in each velocity peak, the conclusion follows that the gas in each velocity peak is much larger in extent in the directions perpendicular to the line of sight than it is parallel to the line of sight. This gas, then, resides in two *sheetlike* structures. The sheets apparently are of greater extent in longitude than in latitude and extend beyond the boundaries of the observed region. The width of the rifts is about 20 pc. If the width of the sheet along the line of sight is also 20 pc, a typical density in each sheet is 2 hydrogen atoms/cm^3. Of course, the sheets could be thinner. For example, if their width were 1 pc they would be nearly bound by self-gravitation; the typical rms velocity of a sheet is 1.4 km/sec, i.e., u (for definition see Fig. 11) $\simeq$ 2 km/sec.

We tentatively attribute the existence of similar rifts in each sheet to a common physical cause and inquire as to its geometrical structure. The gas in the two sheets is separated along the line of sight; the intersection in space of each of the sheets and the physical cause is a linear rift. We conclude that the geometrical structure of the physical cause must also be sheetlike, twisting through space and cutting through the gas in each sheet; both the gas and the disturbance, then, are in the form of sheets. At the higher galactic latitudes, near the tops of the maps in Figure 7, the rifts in the two sheets approach the same position on the sky; this may indicate that there the two sheets are closer together than at lower latitudes.

The maps in Figure 5 imply that the two velocity sheets merge in velocity for $l < 110°$ and that this merged feature then disappears near longitude 102°. This appearance implies that the two sheets are *physically* associated in this region, not that they just happen to have the same velocity; otherwise the disappearance of both sheets at the same longitude would be quite improbable. Here, then, they not only have the same velocity, but they also occupy the same volume of space. If elsewhere the sheets are receding, they could (for example) be considered as a spherical expanding shell or shock; this region would then be that in which the shell is seen tangentially, and the angular width of this region, about 10°, would imply that the thickness of the sheets is about 100 pc instead of the 20 pc found above. Instead, if elsewhere they are approaching, this region would be that where the sheets have collided. These two possibilities are shown schematically in Figure 8. Possible evidence concerning this question is provided by the shapes of the profiles in this region.

At the boundary of this region, where the sheets actually do merge, the gas in the HVS sometimes shifts suddenly in velocity; large spatial gradients of velocity exist. Within the region the singly peaked profiles are wider and flatter than elsewhere (see Fig. 9); the total half-widths are about 12 km/sec. This behavior favors the possibility that the sheets are approaching and that in this region they have collided. This tentative conclusion is perhaps further substantiated by the fact that dust and a relatively large number of young optical objects are more concentrated near here, in the region where the peaks have merged, than elsewhere; the existence of these objects is unusual and must have some physical cause.

Elsewhere the distance between the two sheets is likely to be compatible with the results of Elvius (1967) and Lodén (1961), who find that the absorbing dust is concentrated at two distances, about 300 and 500 pc (see § III*b*). These distances are not irreconcilable with the fact that the apparent sizes of cloudlets in the two sheets are equal (see below), considering the possible sources of discrepancy.

If the large widths of the profiles in the region where the sheets have merged are due only to thermal motion the temperature is about 2500° K. Such temperatures could be generated in a collision as shown by Kahn (1955) and others. The motions could also arise from turbulence. For both cases the velocity dispersion should become smaller owing to cooling (Takayanagi and Nishimura 1960) or turbulent dissipation (time scale for decay = length/velocity dispersion), both of which operate on a time scale of several million years under these conditions. The observed properties of this gas would then be in a transient state and not characteristic of typical interstellar conditions. Alternative-

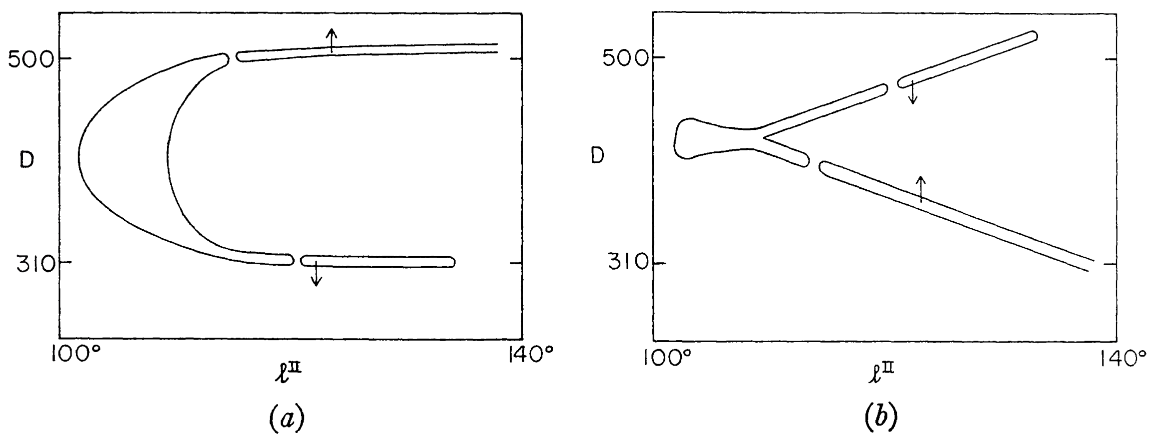

FIG. 8.—Schematic pictures of the probable distribution in distance (*D* in parsecs) and longitude of the two sheets. Only indirect information as to whether the sheets are approaching or receding is available; the HVS is pictured as being further than the LVS in Fig. 8*a*, and conversely in Fig. 8*b*, by the placement of the rifts.

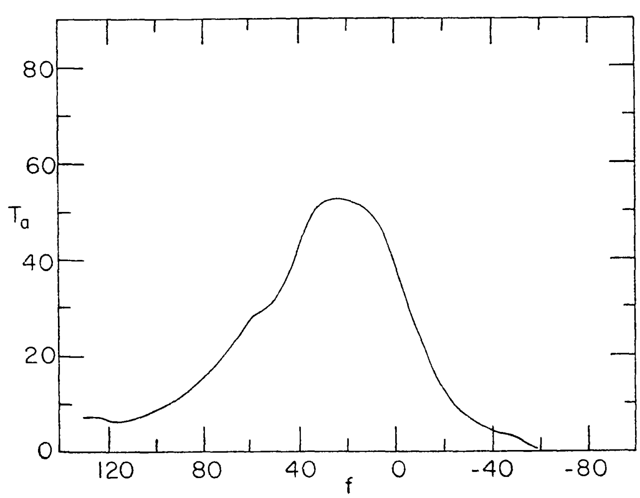

FIG. 9.—Typical profile (antenna temperature, T_a, versus frequency, *f*) in the region where the two velocity sheets have merged, taken at $\delta(1965) = 71°20'$, $\alpha(1950) = 21^h23^m.5$ ($l = 107.94$, $b = 14.95$).

ly, some of the dispersion could be a result of line saturation. If so, the kinetic temperature could be as low as 52° K and the atomic density could be increased by several orders of magnitude over that given in Table 1, where the parameters of the object formed by this merged profile are given (concentration 12) assuming the 21-cm optical depth is small.

b) The Background Component

The portion of the profile due to the background is visible for $l < 97°$ on Figure 5 and where the two velocity components predominate on Figure 5 it is visible as the principal contributor to the antenna temperature between the two components (see also Fig. 1). It is possibly asymmetric, rising more rapidly near zero velocity than on the high-velocity side. Its strength increases with decreasing galactic latitude. It usually changes slowly with position, but near the high-longitude end of the region it disappears along with the high-velocity peak.

The background may be of the character of the broad, weak Gaussian components in WTB's profiles, whose average velocity is roughly that expected from differential galactic rotation (Blaauw 1962; Takakubo 1963; Takakubo and van Woerden 1966). It may be the high-temperature component interpreted by Shuter and Pulley (Costain 1966). Because this background exhibits little, if any, small-scale structure, its gas must be distributed quite uniformly along the line of sight. That its structure is composed of discrete clouds is impossible unless these clouds are much more numerous and tenuous than in the classical cloud model.

A fairly close approximation to the background profile as inferred from the data near $l = 130°$ is given by

$$T_a = 20 \exp\left\{-\left[\frac{(v+6)}{8}\right]^2\right\}, \tag{7}$$

where T_a is the antenna temperature. If caused by differential galactic rotation, the mean velocity of -6 km/sec then implies an average distance of about 400 pc. Using the basic relation for optically thin hydrogen $N_{\rm H} = 1.84 \times 10^{18} \int T_b\, dv$ (see van de Hulst *et al.* 1954), where $N_{\rm H}$ is the number of hydrogen atoms/cm^2 in the line of sight, T_b is the brightness temperature, and v is velocity in km/sec, we find a mean density of about 0.2 hydrogen atoms/cm^3 by assuming all of the velocity dispersion to arise from differential galactic rotation. This is in approximate agreement with the "intercloud" density of 0.1 atoms/cm^3 obtained by Strömgren (1948) from optical absorption line spectra.

The error in this result should be considered very large—the basic concept may be even qualitatively incorrect—because several contradictions are present: (1) More of the velocity dispersion could be thermal or turbulent. (2) The apparent velocity of the background should approach zero as the galactic latitude increases if differential galactic rotation is dominant. (Although the apparent velocity of the background does vary with galactic longitude in the expected manner, this behavior is not pronounced.) Finally, a large amount of optical extinction is associated with the more distant material (§ III*b*), more than is allowed by the observed amount of hydrogen in either sheet according to the argument in § V*f*. If this extinction is due to dust associated with the background component, the background is concentrated within a relatively small distance range. If so, it may be associated with one of the sheets; the nearly simultaneous disappearance of the background and the high-velocity peak suggests that, if this were the case, the background would be associated with the high-velocity sheet. The optical data on the distance of the more distant absorbing component disagree, however, which may indicate that this component has a considerable spread in distance; this possibility would be consistent with a low-density background component which might not be associated with either sheet. Evidently, further optical and radio observations, spread continuously throughout a larger region than has been observed here, are necessary.

c) *Concentrations of Gas*

In Figure 7 are seen several concentrations of gas. For descriptive purposes these concentrations should probably be designated by the term "clouds"; but for reasons stated above, and because their density is not more than about twice that of their surroundings, they are probably not standard interstellar clouds so that we shall call them "concentrations." One of these objects, concentration 9 in Table 1, is visible on Figure 1 in the low-velocity peak for right ascensions between 00^h30^m and 02^h30^m. Rotational motion, which is a linear change of velocity with position and which would be immediately obvious on the original contour maps of antenna temperature versus velocity and right ascension, is small for all concentrations.

TABLE 1

PARAMETERS OF GAS CONCENTRATIONS

Concentration	l	b	Velocity of Concentration (km/sec)	Radius (pc)	$M/M_\odot$	n_H (cm^{-3})	u* (km/sec)	β	u/u_s	β_T
1†........	129.6	13.6	−11	7	280	4	3.6	0.005	3	0.05
2†........	128.3	12.5	−17	11	1200	6	3.0	.02	2.5	.12
3†........	126.0	13.5	−15	8	430	5	4.5	.003	2	.02
4‡........	113.5	11.0	− 9	10	1400	8	4.2	.01	4	.2
5‡........	112.0	13.3	−11	15	4000	7	4.2	.03	2.5	.16
6‡?.......	113.0	12.5	− 4	10	3500	2.1	1.2	.04	1	.04
7.........	131.5	15.5	−11	13	1000	2.7	3.9	.009	2	.03
8.........	119.0	14.5	−12	15	1400	2.7	4.2	.01	2	.04
9.........	125.0	15.5	− 1	36	5000	0.7	2.4	.04	1.5	.1
10.........	106.0	15.0	+ 1	11	4000	2.0	1.7	.02	2	.09
11.........	106.0	17.0	− 6	20	6000	4	3.9	.03	3.4	.38
12§........	106.0	12.5	−11	40	16000	1.5	3.9	.04	3.4	.5
13‖........	125.0	37.0	+ 6	15	2800	5	3.7	0.02	2	0.09

* See Figure 11 for definition.
† In group 1.
‡ In group 2.
§ Merged profile.
‖ Isolated (§V*h*).

The properties of these objects are listed in Table 1, and follow from the following relations concerning the radius R in parsecs, mass M in solar masses, density n_H in hydrogen atoms/cm^3, and β = the ratio of gravitational potential energy for a uniform sphere to twice the kinetic energy $= GM/5R\langle u^2\rangle$, where $\langle u^2\rangle$ is the (observed) one-dimensional random velocity dispersion in km/sec (the virial theorem states that β is unity in gravitational equilibrium):

$$M = 60\int\int N_H dl db\,, \qquad R = 8.75(\Delta l^2 \cos^2 b + \Delta b^2)^{1/2}, \qquad n_H = 6M/R^3,$$
$$\beta = 0.86 \times 10^{-3} M/R\langle u^2\rangle\,. \tag{8}$$

The hydrogen has been assumed optically thin, the possible presence of molecular hydrogen has been neglected, and the objects have been taken as spherical. The expression for the mass includes elements other than hydrogen; hydrogen comprises 63 per cent of the total mass in Population I objects according to Allen (1963). The distance of 500 pc derived above has been assumed. The galactic coordinates, l and b, should be expressed in degrees and the number of atoms/cm^2, N_H, should be expressed in terms of the contour units on Figure 7, 6×10^{19} atoms/cm^2.

Self-gravitation is completely negligible in these objects. But some of them are so large that tidal effects from the z component of the galactic gravitational field, which increases nearly linearly with z in this region (see Oort 1965), helps to contain the objects. This may influence their equilibrium if the net downward gravitational force is balanced by another upward force; for example, this may be responsible for the form of concentrations 8 and 9. Such a possibility has been theoretically treated by Parker (1966).

d) Groups of Clouds

Two regions ($l \simeq 128°$, $b \simeq 13°$; $l \simeq 113°$, $b \simeq 13°$) in the HVS are each best described as a group of clouds superposed on a smoother background of excess density. The properties of these "group clouds" within each group are given in Table 1 (concentrations 1–3 belong to the first group; concentrations 4–6 to the second). One of these is visible in Figure 10 near right ascension 22^h30^m, velocity −10 km/sec.

Self-gravitation is relatively unimportant in the group clouds because both β and β_T are so small; since β varies only linearly with the assumed distance, the values should be fairly reliable. (The quantity β_T is calculated under the assumption that $\langle u^2 \rangle$ is given by the velocity dispersion of cloudlets within the group cloud, the large velocity dispersion observed for the group cloud being due to systematic [e.g., radial] motion; see below.) The observed group clouds are similar to the clouds observed in radio absorption spectra in the galactic plane by Clark *et al.* (1962) and Clark (1965), but less dense. This may be a selection effect, since absorption spectra highlight cold clouds of large optical depth. They are similar to, but somewhat larger and denser than, those found by Dieter (1964, 1965) near the galactic poles. They are similar to "standard interstellar clouds."

Cloudlets (§ V*e*) apparently reside within these objects. The velocity dispersion of a group cloud is usually two or three times that of its associated cloudlets. One might suppose the excess velocity dispersion in these group clouds to be due to temperature or small-scale turbulence. Their cloudlets would then have to be considered as low-temperature regions or as quiescent, turbulence-free regions. The former possibility seems unlikely in a static large cloud because no thermal instabilities exist in the interstellar gas if its density is larger than about 0.3 atom/cm^3 (Field 1962) and the densities inside the clouds are much larger than this value. The latter seems unlikely because quiescent regions inside turbulent material should occur rarely, if ever.

The remaining possibility is that the apparent velocity dispersion of the group clouds is due to large-scale, macroscopic motion. If this motion is so ordered that the velocity difference between two points increases approximately linearly as their distance, a structure such as a cloudlet, which is small compared to a group cloud, can have a velocity dispersion not much larger than thermal. Furthermore, if the velocity in the group cloud is further ordered so that it is purely radial, the cloudlets will never break up simply from kinematical effects because the distance between two moving mass points never becomes very large. On the other hand, a less well-organized velocity field will destroy cloudlets by kinematical effects; the interaction between radial motion and angular motion, for example, results in complicated mass motions inside a contracting large cloud. If, then, the apparent velocity dispersion of a group cloud is caused mainly by radial motion, and if an upper limit to the thermal velocity dispersion is given by the apparent velocity dispersions of the cloudlets imbedded within it, the quantity β must be recalculated. This is the motivation for the calculation of β_T. The author is currently studying the dynamics of this situation; preliminary results indicate that such objects with large radial motion will eventually collapse (Heiles 1966*b*), possibly forming stars or a small dust cloud (see § V*f*).

A further observational attempt can be made to verify this possibility. If the apparent velocity dispersion is due mainly to radial motion, it should become smaller as the edge of the cloud is approached; while otherwise it should be independent of position within the cloud. With the present data such an analysis yields inconclusive results because the spacing of the scans in declination at the positions of the group clouds, all

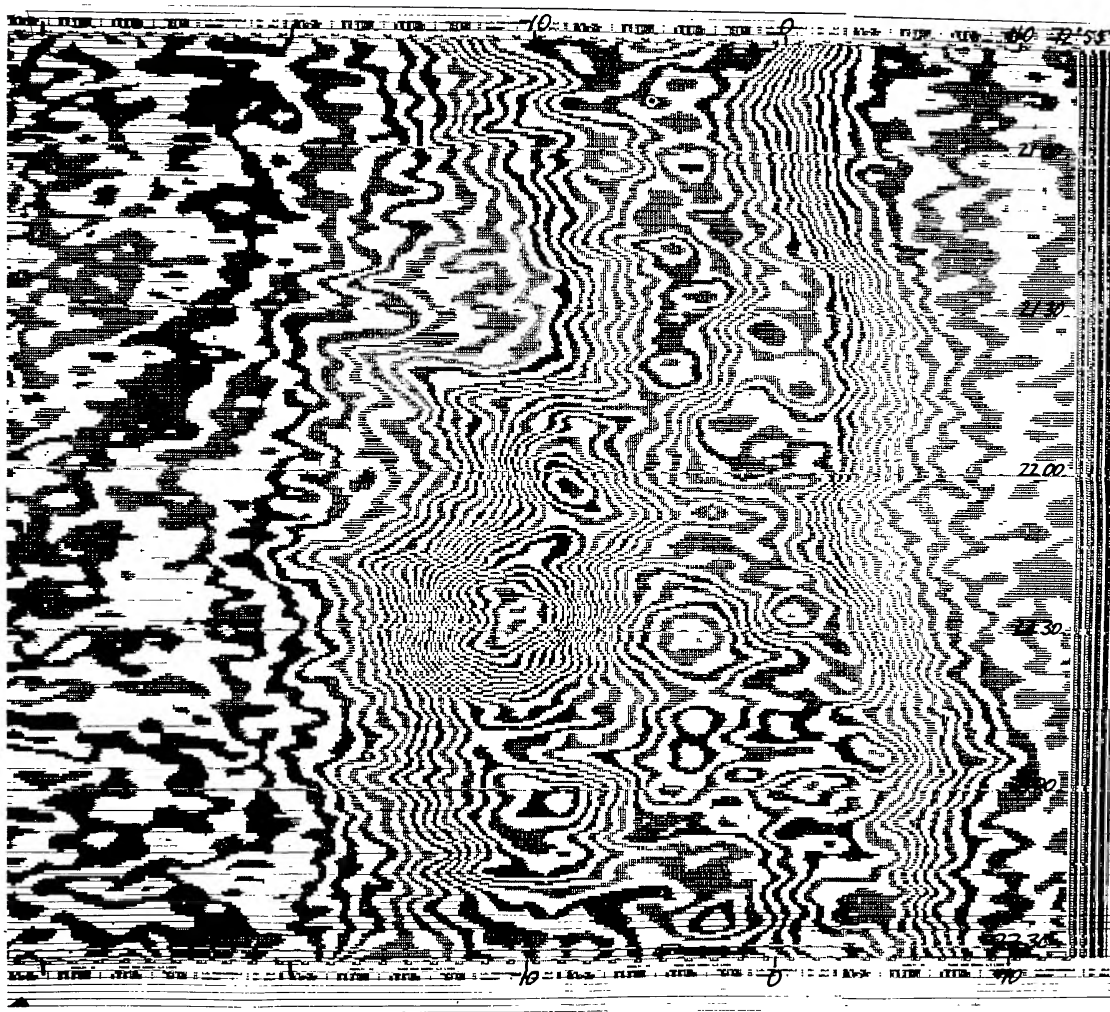

FIG. 10.—Contour map of constant antenna temperature versus right ascension and velocity for a scan which extends beyond the lower latitude boundary of 13° of the observed region. The contour interval (half the temperature difference between two black lines) is approximately 3°04. The two sheets merge suddenly near right ascension 21^h40^m and the nearby structure of the sheets is not typically distinct. Near right ascension 22^h30^m and velocity −12 km/sec appears a group cloud, concentration 5. See the caption of Fig. 1.

of which lie near or off of the edge of the observed region, is usually 1° instead of the usual 5′. Although this in itself is not sufficient to thwart application of the procedure, the existence of cloudlets in these objects (see Fig. 10) necessitates using a complete, detailed map of the entire object since the cloudlets affect a determination of velocity dispersion using only one or two scans. It is important to obtain detailed maps of these and similar regions with a large telescope.

e) Cloudlets

Another structural component of the hydrogen is the small cloudlets which appear nearly everywhere in the two velocity peaks discussed above; they almost never appear in the background component. The cloudlets appear to be immersed in the slowly varying substratum of the velocity sheets. Sometimes they appear to coalesce, probably because their number density is quite high. Many typical cloudlets are visible on Figure 1; those visible on Figure 1, usable for statistical purposes, are listed in Table 2.

The cloudlets within those group clouds having a very high antenna temperature sometimes appear to produce larger antenna temperatures themselves. Their internal velocity dispersions seem larger than those of typical cloudlets, but the dispersions are smaller than those of the clouds in which they are imbedded (see Table 1). The velocity distribution of the cloudlets within such a cloud is similar to the velocity dispersion of the cloud. Undoubtedly too few small, weak cloudlets were found in group clouds where large gradients of antenna temperature with position and velocity exist.

The velocity of most of the cloudlets is confined to the velocity range within the velocity sheets. However, some cloudlets are approaching significantly faster than the hydrogen in the HVS; no objects are receding on the corresponding side of the LVS. Three such objects can be seen on Figure 1 near right ascensions 23^h30^m, 00^h00^m, and 01^h00^m; their velocities are about -20 km/sec. This subclass of cloudlets is characterized by a larger velocity dispersion and sometimes a higher central antenna temperature and a larger angular size than the majority of the cloudlets. Nevertheless, they have been included in the distributions shown in Figures 11 and 12.

No reliable case of hydrogen self-absorption due to cloudlets was observed; apparent cases, such as can be seen at right ascension 01^h30^m and velocity -17 km/sec on Figure 1, can be reliably interpreted as caused by a lack of cloudlets at a particular velocity and position. Self-absorption has been suspected for large-scale hydrogen in the galactic plane by some workers (see Clark 1965).

The excess central temperatures, velocities, velocity widths, and angular sizes of 815 cloudlets were measured. Often cloudlets appear to coalesce; the measurements were accepted only if a particular cloudlet was distinguishable from the surrounding cloudlets. A cloudlet was accepted as real, not simply noise, only if it was visible on at least three neighboring contour maps (scans were usually separated by 5′ in declination). Because of blending the true number of cloudlets in the regions is larger than the number measured, perhaps by a factor of 2. The locations of these objects are not shown on a map because the apparent positional distribution is affected by the presence of group clouds, as mentioned above; the 815 objects are scattered roughly uniformly over the observed region, but do not occur in the rifts.

The distributions of mass, density, central brightness temperature, and velocity dispersion (u) are shown in Figure 11; the usual distance of 500 pc was assumed and the surrounding gas, which may permeate the cloudlets, was neglected in the calculations of mass and density. Bivariate distributions of several pairs of variables were attempted; some of these are shown in Figure 12. If the size spectrum of the cloudlets is universal, one expects the angular size to be correlated with the velocity if the velocity is correlated with distance as would occur if differential galactic rotation were important; such a correlation was not observed. Some theoretical interpretations of the interstellar velocity field might expect equipartition in the cloudlets, so that mass and velocity

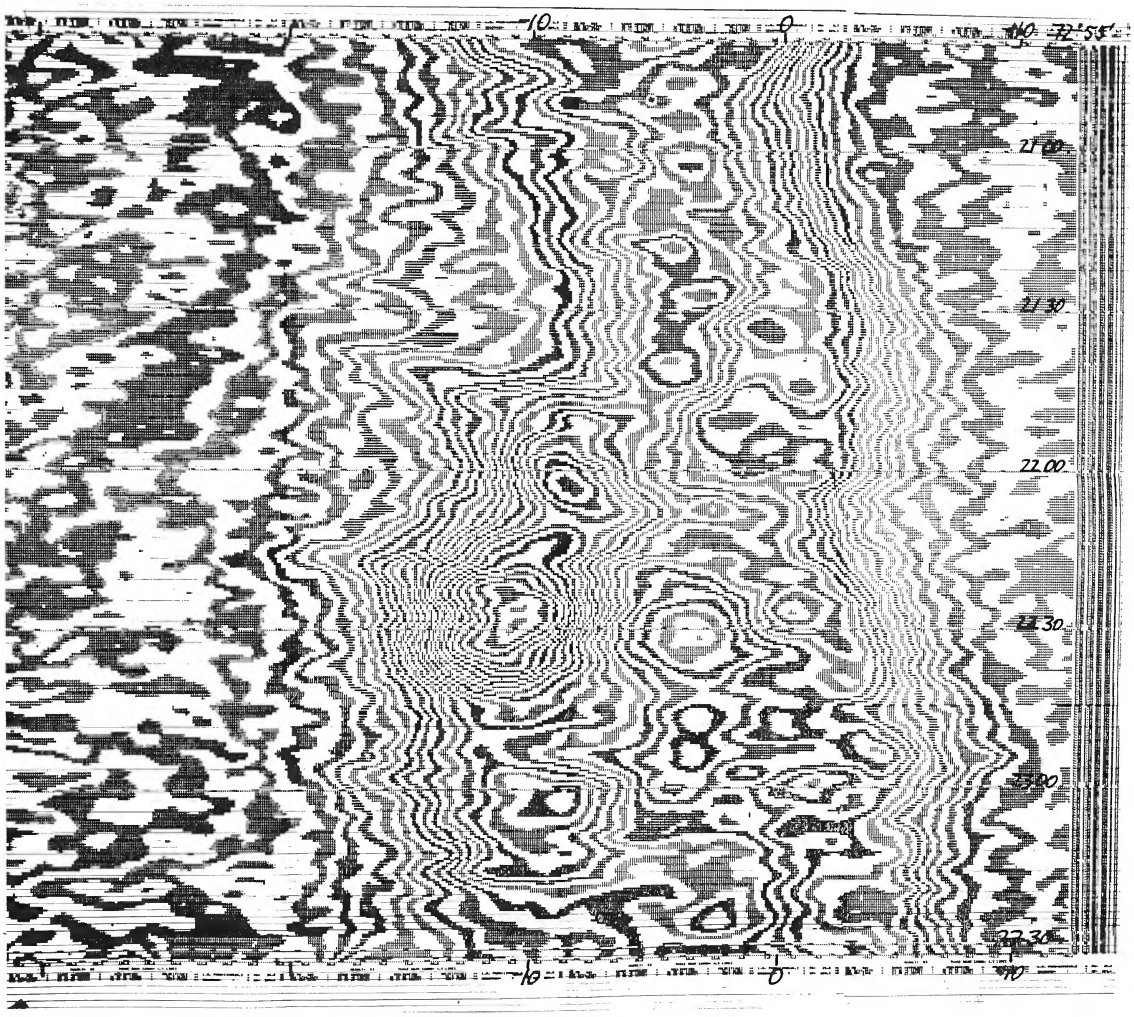

FIG. 10.—Contour map of constant antenna temperature versus right ascension and velocity for a scan which extends beyond the lower latitude boundary of 13° of the observed region. The contour interval (half the temperature difference between two black lines) is approximately 3°.04. The two sheets merge suddenly near right ascension 21^h40^m and the nearby structure of the sheets is not typically distinct. Near right ascension 22^h30^m and velocity -12 km/sec appears a group cloud, concentration 5. See the caption of Fig. 1.

should be correlated; such a correlation was not found. The density within cloudlets varies only a little, according to Figure 11; thus the mass and radius, and $T_c u$ and radius, are well correlated in an obvious fashion (where T_c is the central brightness temperature and u the velocity dispersion; $T_c u$ is proportional to N_H, the number of atoms/cm^2, through the center of the cloudlet). A successful correlation of radius and velocity width was obtained; this correlation, together with the above two correlations caused by the well-defined density in the cloudlets, produces predictable correlations in M and u, and

TABLE 2

PARAMETERS OF CLOUDLETS IN FIGURE 1

δ(1965)	α(1950)	Velocity of Cloudlet (km/sec)	Radius (pc)	$M/M_\odot$	n_H (cm^{-3})	u* (km/sec)
78°07′	23h40m9	+ 0.8	2.9	7.9	1.8	1.3
78 22	23 47.1	+ 4.9	3.0	7.1	1.6	1.3
78 32	23 48.8	−12.7	2.0	1.7	1.4	0.8
78 22	23 59.3	− 9.1	2.0	2.1	1.6	1.0
78 20	23 59.4	−23.0	3.4	24.6	3.6	2.4
78 20	0 1.0	−12.7	2.5	5.8	2.2	1.3
78 35	0 14.6	+ 0.2	3.8	29.5	3.4	1.6
78 00	0 17.5	− 3.6	3.6	10.1	1.4	1.3
78 32	0 18.9	−20.0	2.8	6.2	1.8	1.5
78 27	0 28.4	+ 0.8	1.9	2.1	1.8	0.8
78 40	0 34.5	−17.3	3.7	13.8	1.8	1.2
78 52	0 35.4	+ 0.8	3.2	4.8	1.0	0.8
77 57	0 41.2	+ 1.9	4.5	22.1	1.4	1.2
79 10	0 42.0	−10.1	4.7	21.4	1.2	1.9
77 57	0 54.3	+ 1.9	3.8	11.2	1.4	1.0
78 37	0 58.4	−19.6	2.7	5.0	1.6	1.3
78 15	1 0.2	− 9.5	2.1	4.1	2.8	1.5
78 15	1 1.7	−11.0	2.8	8.8	2.4	1.4
78 17	1 4.0	−13.1	2.1	3.3	2.2	1.2
77 55	1 5.0	+ 1.9	2.7	4.8	1.6	1.0
78 15	1 5.7	− 0.2	2.9	6.0	1.4	0.9
78 22	1 9.1	− 7.0	1.9	1.7	1.4	1.0
78 30	1 10.1	+ 7.0	3.1	7.4	1.6	1.4
78 25	1 16.6	−14.3	2.5	8.2	3.2	1.4
78 22	1 18.2	+ 2.3	2.8	10.6	3.0	1.1
78 22	1 18.6	−20.9	1.9	3.2	2.8	1.3
78 15	1 27.4	− 1.3	4.9	53.9	2.8	1.5
78 20	1 30.0	−11.2	1.5	0.7	1.2	0.9
78 20	1 30.4	+ 0.2	2.9	8.8	2.0	1.1
78 27	1 31.9	−20.5	1.9	2.9	2.6	1.1
78 25	1 35.8	+ 2.5	3.2	16.1	3.0	1.2
78 07	1 36.9	−18.1	3.2	12.7	2.4	1.4
78 25	1 36.9	+ 8.9	2.7	3.2	1.0	0.9
78 32	1 37.2	+ 9.1	2.4	3.4	1.4	1.1
78 12	1 43.8	−15.8	3.1	14.2	3.0	1.3
78 22	1 44.1	−16.2	1.4	1.3	2.8	1.2
78 02	1 46.3	+ 2.3	2.4	6.5	2.8	1.0
78 15	1 52.0	− 3.0	1.8	1.9	2.0	1.0
78 15	1 56.4	+ 6.5	2.5	3.9	1.4	1.0
77 52	1 57.2	−11.8	4.1	15.6	1.4	1.1
78 17	2 2.9	− 0.8	3.4	11.6	1.8	1.2
78 15	2 6.7	−11.0	2.3	4.4	2.2	1.3
78 12	2 14.5	− 7.0	2.9	6.1	1.4	1.4
78 05	2 17.9	−15.2	2.4	3.1	1.4	1.0
78 30	2 23.5	− 9.9	2.3	2.4	1.2	1.1

* See Fig. 11 for definition.

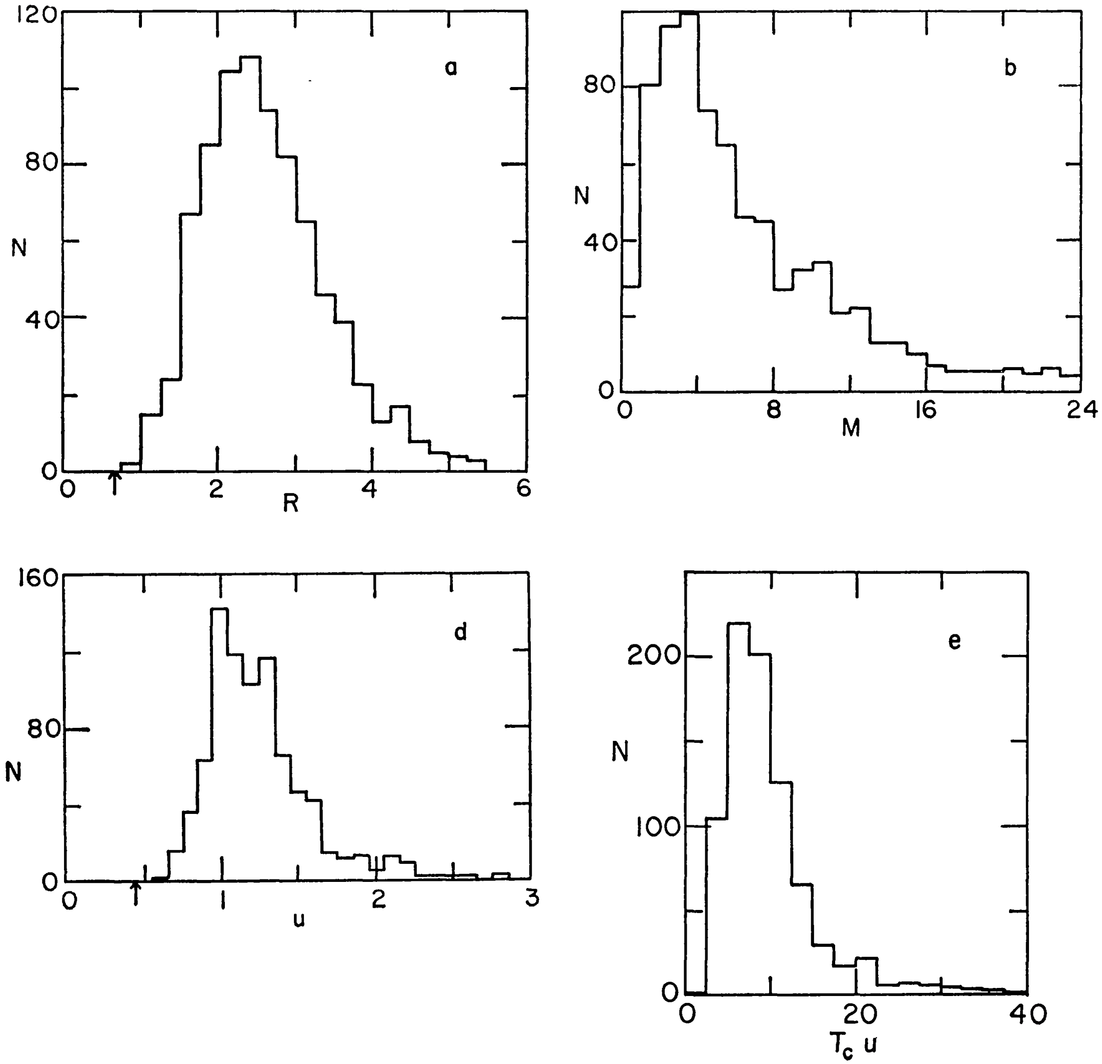

FIG. 11.—Distributions of parameters characterizing cloudlets. The units are: R, parsecs; M, solar masses; n_H, hydrogen atoms/cm^3. The mass and density are calculated assuming the cosmic abundances as given by Allen (1963); u is the velocity width in km/sec, taking the velocity distribution as exp $-(v/u)^2$; the value of u of the receiver passband is 0.63 km/sec. The central brightness temperature, T_c, is in degrees. N is the number of cloudlets observed having the identicated value of the parameter. The arrows represent the instrumental resolutions (the brightness temperature sensitivity depends on declination and cloudlet size so is not a uniquely defined quantity; an average value is shown); none of the measured quantities has been corrected for these instrumental effects.

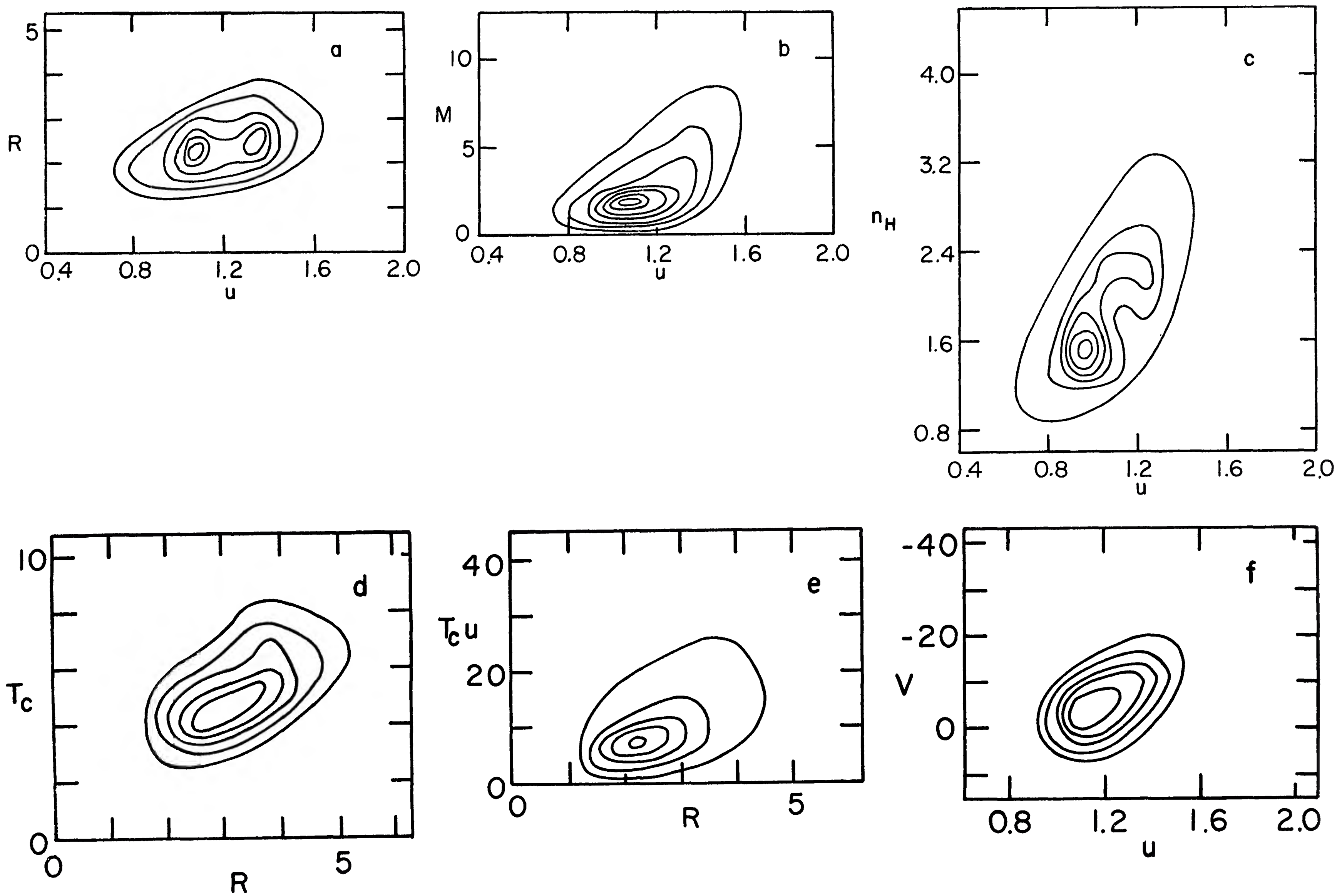

FIG. 12.—Some bivariate distributions of parameters characterizing cloudlets. In figures with unlabeled contours the contour interval is constant. The units for all variables are the same as quoted in the legend for Fig. 11. The shapes of the bivariate distributions of mass and density with respect to R can be obtained by magnifying the scale of Tu in Fig. 12e by R^2 and R^{-1}, respectively. Fig. 12f, showing the bivariate distribution of velocity and velocity dispersion, is only for those cloudlets in the merged velocity profile (see text); the bivariate distribution of these parameters for the other cloudlets shows no correlation.

$T_c u$ and u. Of course, some of these correlations are simply due to interrelations between parameters. An unexpected correlation in the low-longitude part of the region, where the two velocity components merged, was found for v, the velocity of the cloudlets, and u; these quantities are uncorrelated elsewhere.

The distribution of central brightness temperature in Figure 11 is of observational interest, because it is evident that the instrumental sensitivity affects this distribution. In this connection we note the bivariate distribution of T_c and R in Figure 12, which indicates a linear relation between the two variables and is readily understandable on consideration of the well-defined density and velocity width for the cloudlets. This correlation reveals that smaller temperatures are produced by smaller cloudlets. This relation is such that, when considering cloudlets of decreasing size, T_c decreases below the temperature sensitivity before the angular size decreases below the angular resolution limit. Thus the effective spatial resolution is limited by instrumental noise, not by the antenna beam width: smaller scale structure, if it exists, can be seen only by using observing techniques significantly more sensitive than those used here. The author is currently planning further observations, using another technique, to explore this point.

We note that the ranges of variation of density, radius, and internal velocity dispersion of cloudlets are fairly small. The cloudlet excess density is about twice that of the background gas of the sheets, in which they are imbedded. The internal velocity dispersion, typically equal to 1.2 km/sec, yields an upper limit on the temperature of the gas of about 100° K. Self-gravitation of the cloudlets is a completely negligible binding force unless molecular hydrogen is several hundred times more abundant than atomic hydrogen, and for this reason they might be expected to disperse very quickly. However, their profusion indicates that they are probably stable objects. A possible situation, consistent with all observational evidence, is that they are cool objects in pressure equilibrium with their surroundings; the estimates of density in the sheet and in the cloudlets, together with the smaller internal velocity dispersion of the cloudlets relative to that of the sheets, make this model reasonable. Alternatively, they might be true turbulence elements.

We note that cloudlets may have already been observed in the absorption spectrum of the Orion Nebula by Clark *et al.* (1962) and in optical interstellar spectra by Hobbs (1965; private communication); both sets of data show absorption lines of velocity width similar to that of our cloudlets, although the number of these narrow lines seems smaller than expected on the basis of the present data. We also note that the frequency distributions of the Gaussian components of intermediate-latitude hydrogen-line profiles made from the lists of Takakubo and van Woerden (1966) are completely different from those for the cloudlets. This is, of course, partly because their distributions refer to all of the hydrogen seen in a profile, whereas ours refer only to the cloudlets.

G. Field (private communication) has pointed out that the mass spectrum of the cloudlets is well approximated by an inverse-square power law over the range 6–20 $M_\odot$, consistent with Salpeter's (1955) initial luminosity function for stars which also can be fitted fairly well over the range 9–25 $M_\odot$ by an inverse-square power law. Further observations with better sensitivity are required for reliable extension of the cloudlet mass spectrum.

f) Clouds of Dust

In Figure 3 are indicated the positions of the dust clouds and diffuse nebulae mentioned above. Upon comparison with Figure 7, we find weak if any correlation of the hydrogen distribution with the dust distribution. The lack of correlation is especially evident for some of Lynds's clouds.

This is surprising in view of the current evidence that the optical extinction is produced by classical dielectric spheres (see Greenberg 1966). Since classical dielectric spheres are solid grains composed principally of heavy elements (van de Hulst 1949) the total mass of grains relative to that of hydrogen can be only slightly larger than the relative abundance of heavy elements. A given optical extinction results in a lower limit for the projected mass density of grains. Heavy elements comprise about 1.4 per cent by mass of typical Population I material, according to Allen (1963); thus a given optical extinction also results in a lower limit for the amount of hydrogen along the line of sight, except in the unlikely circumstance that hydrogen is severely depleted relative to heavy elements. This in turn results in a lower limit of the area under a line profile if the 21-cm optical depth is small:

$$\int T_b dv \geq 430\ \Delta m\ ,$$

where v is in km/sec and Δm is the extinction due to dust in magnitudes. The relations of Lilley (1955) have been used to obtain this approximate equation. Equality corresponds to the case in which all of the heavy elements have condensed into the grains; the introduction of graphite grains (see Hoyle and Wickramasinghe 1962) changes this equation by only a small factor. We again note that the general interstellar medium corresponds approximately to equality—so that in typical interstellar gas nearly all of the heavy elements are contained by the dust. Lynds's clouds are obvious upon casual inspection of even the red Palomar prints and, therefore, have absorptions of at least 1 mag. Since their size is comparable to that of the antenna beam the antenna temperature is approximately equal to the brightness temperature, so that equation (9) predicts integrated brightness temperatures larger than the entire area under a typical profile (cf. Fig. 1). Of course, this prediction is not fulfilled, particularly for Lynds's clouds. Bok, Lawrence, and Menon (1955) and Davies (1958) have noticed a similar discrepancy for other clouds, and Garzoli and Varsavsky (1966) find complete disagreement with Lilley's law in an optically unusual region in Taurus (see Heiles 1967). Three possible causes of these discrepencies are: (1) a large chemical abundance anomaly, in the sense that the relative abundance of hydrogen is about $\frac{1}{100}$ its normal value; (2) the hydrogen is cold or molecular in form; (3) the absorption is not due to classical dielectric spheres. We immediately dismiss (1) as being implausible, and consider the second and third possibilities.

We discuss quantitatively the three dust clouds near $l = 114°$, $b = 15\overset{\circ}{.}5$ as specific examples. From the extinction, which we take as 1 mag, and the observed radius of about 2.2 pc (the usual distance of 500 pc has been assumed) we find each of these clouds has a mass of 110 solar masses and a density of 1.5×10^{-22} g/cm^3 if all of the heavy elements are bound in classical dielectric spheres of radius 3×10^{-5} cm. Under these conditions the gas is expected to be very cold, both because the dust shields it from galactic radiation, thus removing the most important heating source, and because the cooling time is very short, about 10^5 years (Takayanagi and Nishimura 1960), at these densities. Such cold, dense hydrogen atoms would produce a profile whose maximum antenna temperature would be somewhat less than the kinetic temperature (the exact value depends on the size of the objects through eqs. [1] and [2]) and which could be broad from saturation effects. Similar considerations have been advanced by Davies (1958). Such a profile could easily go unnoticed, being imbedded among the data from the other hydrogen in the line of sight; however, the low-velocity hydrogen surrounding these features does not appear to produce an unusual profile.

Although the presence of extremely cold hydrogen atoms cannot be unequivocally ruled out on observational grounds, theoretical discussions (McCrae and McNally 1960; Gould and Salpeter 1963) predict that under these conditions molecular hydrogen would form rapidly by association on the grains. The time scale for this process is about 10^7 years under the conditions quoted above. On the other hand, the opacity of the dust may be large enough to depress the grain temperature sufficiently so that they accrete frozen hydrogen (Gould and Salpeter 1963). In any event, then, it is not surprising that few hydrogen atoms are observed to be associated with these dust clouds, even though the amount of hydrogen actually involved should be very large. Garzoli and Varsavsky

(1966) arrive at similar conclusions. The recent discovery of normal OH emission from dust clouds (Heiles 1968) reinforces these conclusions.

We now consider the self-gravitation of these clouds of matter. We assume no external pressure, an equilibrium temperature of 15° K, and the mass and radius quoted above. These conditions are not biased to overestimate the importance of self-gravitation relative to the expected real conditions, because the optical extinction is actually larger than 1 mag. The resulting value of β is somewhat larger than unity, which indicates that self-gravitation is a dominant binding force in these objects. These are the only interstellar structures observed here in which self-gravitation is important. Any such object will collapse at a rate determined by its radiation rate and systematic velocity field; thus, these objects seem to be particularly good candidates for future regions of star formation.

The above discussion is nonsense, of course, if the grains are not classical dielectric spheres but instead are more efficient absorbers—for example, the particles less than

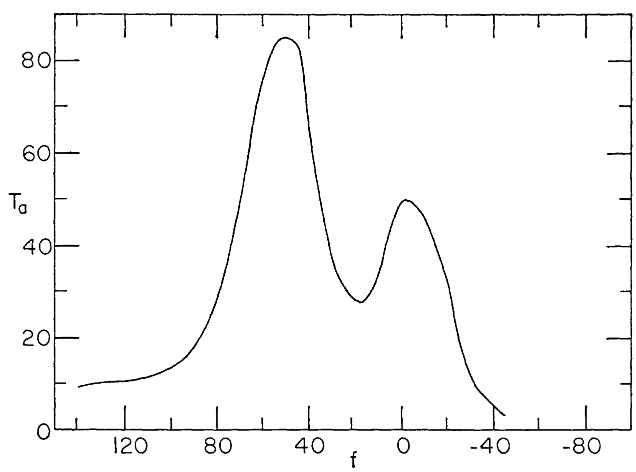

FIG. 13.—Profile (antenna temperature, T_a', versus frequency f) in which the highest brightness temperature was found, taken at $\delta(1965) = 72°55'$, $\alpha(1950) = 22^h27^m.5$ ($l = 112.90$, $b = 13.06$).

10 Å in radius proposed by Platt (1956). A given absorption in this case requires much less total mass than does the same absorption by classical grains. Since the expected amount of hydrogen atoms is correspondingly reduced if the chemical composition remains constant, no discrepancy with the present observations would occur.

In this case the total amount of mass associated with the clouds is not unusual, and one wonders why the absorption is so concentrated in space. On the other hand, the mass requirement associated with classical dielectric particles provides a mechanism for the production of the particles (atomic collisions at low temperature and high density) and provides the necessary gravitational field to hold the objects together. This state of affairs seems more self-consistent.

g) *The Highest Brightness Temperature*

The value of the highest brightness temperature observed in the region is of interest only because it is about 130° K, equal to the commonly used value for the kinetic temperature of interstellar hydrogen in the Galaxy. This temperature occurs in concentration 7. The corresponding line profile is shown in Figure 13 (from the size of the object, η was estimated to be 0.6; see eq. [3]); since the position of this line profile lies outside of the well-observed region, where scans were separated by 1° in declination, the brightness temperature probably rises even higher at a neighboring declination. The profile does not seem to be particularly saturated: we conclude that the actual hydrogen kinetic temperature is significantly greater than 130° K.

Since line profiles taken in the galactic plane saturate near 125° K, we are confronted with definite evidence for temperature variations in interstellar hydrogen. Previous work also indicates kinetic temperature variations. Low temperatures, near 35°, have been found by Williams (1963) and Clark (1965); high temperatures, several hundred degrees, have been found by Shuter and Pulley (Costain 1966).

h) An Isolated Concentration

On an auxiliary scan (Fig. 4) an isolated concentration was found near $l = 125°$, $b = 37°$. The structure within this isolated cloud is very similar to the structure within the high- and low-velocity peaks found in the well-observed region; this indicates that the measurements of cloudlets in the well-observed region are not significantly affected by blending with other hydrogen in the line of sight. The parameters of this isolated cloud, as inferred from this single scan, have been indicated in Table 1 (concentration 13).

VI. DISCUSSION AND SUMMARY

The preceding section is the author's interpretation of the data. As such it is necessarily a simplification and condensation of the true situation. In particular, many interesting individual features exist; especially interesting is the region in which the two sheets merge, for fascinating structure and rapidly varying velocity fields exist there (e.g., right ascension 21^h45^m in Fig. 10) which are not described by concepts presented above. Full appreciation and understanding of the situation require at least a cursory look at the original data.

Two of the most surprising and important results of this investigation are the lack of agreement with the standard cloud model and the apparent importance of the large-scale structure which carries much of the mass and whose velocity varies only slowly with position—in short, a much different *qualitative* picture from previous ones. Should these general characteristics be confirmed as being typical of the interstellar gas the ramifications would be great: the cloud model with its huge energy requirement has served as the very basis for much of the theoretical work on the interstellar medium during the last decade.

On the largest scale this structure consists of the smooth background component, which by far contains most of the hydrogen. Its velocity probably depends on galactic coordinates in the way expected for interstellar matter, and it has little spatial structure. In addition, we have the two sheets, which are in relative motion (probably approaching) and are connected at one end of the region. Their velocities cannot be used as distance indicators. Within each sheet exist various concentrations; these can be seen in Figure 7 which is a "photograph" of the projected hydrogen density as a function of position for each sheet. Individual concentrations within each sheet do not seem completely independent, but rather appear related and connected together in some loose sense. The dimensions involved are huge; eye estimates of typical correlation angles yield larger than 5°, or about 50 pc.

Within the sheets appear the rifts, in which the neutral hydrogen of each sheet is absent. Within the sheets also appear smaller concentrations, the group clouds. These objects are similar to "standard interstellar clouds" except that they cluster together and probably most of their observed velocity dispersion is systematic radial motion.

On a still smaller scale we have the cloudlets, imbedded everywhere in the sheets and about three times as dense as the sheets. The detection of small cloudlets is hindered by instrumental sensitivity, not antenna beam width. The cloudlet mass spectrum simulates that a newly born stars. They may be cool pockets in pressure equilibrium with the surrounding gas in the sheets, or turbulence elements. On a still smaller scale are dust clouds, which are definitely very dense objects in which all of the hydrogen is probably molecular. These objects are bound by self-gravitation and thus may be regions of future star formation.

Finally we repeat two unrelated but important and unusual facts. The first is the highest observed brightness temperature, at least 130° K, larger than the commonly accepted value. The second is the rapid decrease in projected density with galactic latitude for both the background and the sheets, and particularly the extremely rapid cutoff in the projected hydrogen density near galactic latitude 28°.

Can the present region be regarded as typical so that these results can be extrapolated to the general interstellar medium? The present region comprises only about 0.5 per cent of the area of the sky, and seems to be an atypical one at that; thus the a priori answer is definitely "no": further observations are planned to establish this point.

Dr. George Field originally suggested the need for observations of this type and was very helpful throughout the work. Dr. Gart Westerhout was instrumental in the development of the receiver to perfection and was in other respects of great benefit to the author. Dr. Lyman Spitzer served as my thesis adviser during the latter stages. Dr. Harold Weaver kindly read the manuscript and offered several suggestions.

The success of this project relied on the superb facilities of the National Radio Astronomy Observatory. It is a great pleasure to acknowledge the assistance and hospitality of the entire staff, and in particular to thank Dr. D. S. Heeschen for the use of the facilities.

Throughout most of this work support was provided by the Peyton Fellowship of Princeton University. The National Radio Astronomy Observatory generously provided support during two summers; for the last four months of the project support was provided by Air Force contract AF49 (638)-1555.

REFERENCES

Adams, W. W. 1949, *Ap. J.*, **109**, 354.
Allen, C. W. 1963, *Astrophysical Quantities* (London: Athlone Press).
Baars, J., and Mezger, P. 1964, Electronics Division Internal Rept. No. 30, National Radio Astronomy Observatory, Green Bank, W.Va.
Batchelor, G. K. 1963, *Homogeneous Turbulence* (Cambridge: Cambridge University Press).
Bennett, A. S. 1961, *Mem. R.A.S.*, **68**, 163.
Berkhuijsen, E. M., and Brouw, W. N. 1963, *B.A.N.*, **17**, 185.
Berkhuijsen, E. M., Brouw, W. N., Muller, C. A., and Tinbergen, J. 1964, *B.A.N.*, **17**, 465.
Blaauw, A. 1962, in *Interstellar Matter in Galaxies*, ed. L. Woltjer (New York: W. A. Benjamin, Inc.), p. 48.
Blaauw, A., Gum, G. S., Pawsey, J. L., and Westerhout, G. 1959, *Ap. J.*, **130**, 702.
Bok, B. J. 1937, *The Distribution of Stars in Space* (Chicago: University of Chicago Press).
Bok, B. J., Lawrence, R. S., and Menon, T. K. 1955, *Pub. A.S.P.*, **68**, 249.
Cederblad, S. *Studies of Bright Diffuse Galactic Nebulae* (Lund, Sweden: The Observatory), 1946.
Clark, B. G. 1965, *Ap. J.*, **142**, 1398.
Clark, B. G., Radhakrishnan, V., and Wilson, R. W. 1962, *Ap. J.*, **135**, 151.
Costain, C. H. 1966, *I.A.U. Symp. No. 31.*
Davies, R. D. 1958, *Rev. Mod. Phys.*, **30**, 443.
———. 1960, *M.N.R.A.S.*, **120**, 483.
Dicke, R. H. 1946, *Rev. Sci. Instr.*, **17**, 268.
Dieter, N. H. 1964, *A.J.*, **69**, 288.
———. 1965, *ibid.*, **70**, 552.
Donn, B. 1958, *Rev. Mod. Phys.*, **30**, 940.
Elvius, T. 1956, *Stockholm Obs. Ann.*, **19**, No. 3.
Erickson, W. C., and Helfer, H. L. 1960, *A.J.*, **65**, 1.
Field, G. B. 1962, in *Interstellar Matter in Galaxies*, ed. L. Woltjer (New York: W. A. Benjamin, Inc.), p. 48.
———. 1965, *Ap. J.*, **142**, 531.
Findlay, J. W. 1963, *Sky and Telescope*, **25**, 68.
Garzoli, S. L., and Varsavsky, C. M. 1966, *Ap. J.*, **145**, 79.
Gould, R. J., and Salpeter, E. E. 1963, *Ap. J.*, **138**, 393.
Greenberg, J. M. 1966, *Ap. J.*, **145**, 63.

Heiles, C. 1966*a*. *Catalog of Hydrogen-Line Data at Intermediate Latitudes* (Green Bank, W.Va.: National Radio Astronomy Observatory).
———. 1966*b*, unpublished Ph.D. dissertation, Princeton University.
———. 1967, *Ap. J.*, **148**, 299.
———. 1968, *Ap. J.*, **151** (in press).
Heiles, C., and Henry, R. 1966, *Ap. J.*, **146**, 953.
Hobbs, L. 1965, *Ap. J.*, **142**, 160.
Hoyle, F., and Wickramasinghe, N. C. 1962, *M.N.R.A.S.*, **124**, 417.
Hubble, E. 1934, *Ap. J.*, **79**, 8.
Hulst, H. C. van de. 1949, *Rech. Astr. de l'Obs. Utrecht*, **11**, Part 2.
Hulst, H. C. van de, Müller, C. A., and Oort, J. H. 1954, *B.A.N.*, **12**, 117.
Kahn, F. D. 1955, in *Gas Dynamics of Cosmic Clouds* (Amsterdam: North-Holland Publishing Co.), p. 60.
Keenan, P. C. 1963, in *Basic Astronomical Data*, ed. K. Aa. Strand (Chicago: University of Chicago Press), p. 78.
Kellermann, K. 1964, *A.J.*, **69**, 205.
Kerr, F. J., Hindman, J. V., and Gum, C. S. 1959, *Australian J. Phys.*, **12**, 270.
Kerr, F. J., and Westerhout, G. 1965, in *Galactic Structure*, ed. A. Blaauw and M. Schmidt (Chicago: University of Chicago Press), p. 167.
Khavtassi, J. Sh. 1960, *Atlas of Galactic Dark Nebulae* (Abastumani Astrophysical Observatory).
Ko, H. C. 1961, Rept. No. 21, Radio Observatory, Department of Electrical Engineering, The Ohio State University, Columbus, Ohio.
Lilley, A. E. 1955, *Ap. J.*, **121**, 559.
Lodén, L. O. 1961, *Stockholm Obs. Ann.*, **21**, No. 7.
Lynds, B. T. 1962, *Ap. J. Suppl.*, **7**, 1.
McCrae, W. H., and McNally, D. 1960, *M.N.R.A.S.*, **121**, 238.
McGee, R. X., and Murray, J. D. 1961, *Australian J. Phys.*, **14**, 260.
McGee, R. X., Murray, J. D., and Milton, J. 1963, *Australian J. Phys.*, **16**, 136.
Maltby, P., and Moffet, A. T. 1962, *Ap. J. Suppl.*, **7**, 141.
Mezger, P. G. 1963, Electronics Division Internal Rept. No. 17, National Radio Astronomy Observatory, Green Bank, W.Va.
Münch, G. 1957, *Ap. J.*, **125**, 42.
Münch, G., and Unsöld, A. 1962, *Ap. J.*, **135**, 711.
Oort, J. H. 1965, in *Galactic Structure*, ed. A. Blaauw and M. Schmidt (Chicago: University of Chicago Press), p. 455.
Parker, E. N. 1966, *Ap. J.*, **145**, 811.
Platt, J. R. 1956, *Ap. J.*, **123**, 486.
Salpeter, E. E. 1955, *Ap. J.*, **121**, 161.
Schlüter, A., Schmidt, H., and Stumpff, P. 1953, *Zs. f. Ap.*, **33**, **194**.
Schmidt, M. 1957, *B.A.N.*, **13**, 247.
———, 1965, in *Galactic Structure*, ed. A. Blaauw and M. Schmidt (Chicago: University of Chicago Press), p. 513.
Seeger, Ch. L., Westerhout, G., Conway, R. G., and Hoekema, T. 1965, *B.A.N.*, **18**, 11.
Shalloway, A. M. 1964, *The NEREM Record.*
Spitzer, L. 1958, *Rev. Mod. Phys.*, **30**, 1102.
———. 1967, in *Interstellar Matter* (Chicago: University of Chicago Press) (in press).
Spitzer, L., and Skumanich, A. 1952, *Ap. J.*, **116**, 452.
Strömgren, B. 1948, *Ap. J.*, **108**, 242.
Takakubo, K. 1963, *Sendai Astr. Raportoj*, No. 85.
Takakubo, K., and Woerden, H. van. 1966, *B.A.N.*, **18**, 488.
Takayanagi, K., and Nishimura, S. 1960, *Pub. Astr. Soc. Japan*, **12**, 77.
Ulam, S. M. 1964, *Sci. Am.*, **211**, No. 3, p. 202.
Weinreb, S. 1963, Tech. Rept. No. 412, Massachusetts Institute of Technology, Research Laboratory of Electronics, Cambridge, Mass.
Williams, D. R. W. 1963, *Quasi-stellar Sources and Gravitational Collapse*, ed. I. Robinson, A. Schild, and E. L. Schucking (Chicago: University of Chicago Press), p. 213.
Woerden, H. van. 1962, doctoral thesis, University of Gronigen.
Woerden, H. van, Takakubo, K., and Braes, L. L. E. 1962, *B.A.N.*, **16**, **321**.